Acta Oceanol. Sin., 2021, Vol. 40, No. 7, P. 100–118
https://doi.org/10.1007/s13131-021-1703-8
http://www.aosocean.com
E-mail: ocean2@hyxb.org.cn

The long-term trend of Bohai Sea ice in different emission scenarios

Donglin Guo[1, 2], Rui Li[2], Peng Zhao[2]*

[1] College of Oceanic and Atmospheric Sciences, Ocean University of China, Qingdao 266100, China

[2] North China Sea Marine Forecasting Center, Ministry of Natural Resources, Qingdao 266061, China

Received 21 July 2020; accepted 22 October 2020

Abstract

Based on a coupled ocean-sea ice model, this study investigates how changes in the mean state of the atmosphere in different CO_2 emission scenarios (RCP 8.5, 6.0, 4.5 and 2.6) may affect the sea ice in the Bohai Sea, China, especially in the Liaodong Bay, the largest bay in the Bohai Sea. In the RCP 8.5 scenario, an abrupt change of the atmospheric state happens around 2070. Due to the abrupt change, wintertime sea ice of the Liaodong Bay can be divided into 3 periods: a mild decreasing period (2021–2060), in which the sea ice severity weakens at a near-constant rate; a rapid decreasing period (2061–2080), in which the sea ice severity drops dramatically; and a stabilized period (2081–2100). During 2021–2060, the dates of first ice are approximately unchanged, suggesting that the onset of sea ice is probably determined by a cold-air event and is not sensitive to the mean state of the atmosphere. The mean and maximum sea ice thickness in the Liaodong Bay is relatively stable before 2060, and then drops rapidly in the following decade. Different from the RCP 8.5 scenario, atmospheric state changes smoothly in the RCP 6.0, 4.5 and 2.6 scenarios. In the RCP 6.0 scenario, the sea ice severity in the Bohai Sea weakens with time to the end of the twenty-first century. In the RCP 4.5 scenario, the sea ice severity weakens with time until reaching a stable state around the 2070s. In the RCP 2.6 scenario, the sea ice severity weakens until the 2040s, stabilizes from then, and starts intensifying after the 2080s. The sea ice condition in the other bays of the Bohai Sea is also discussed under the four CO_2 emissions scenarios. Among atmospheric factors, air temperature is the leading one for the decline of the sea ice extent. Specific humidity also plays an important role in the four scenarios. The surface downward shortwave/longwave radiation and meridional wind only matter in certain scenarios, while effects from the zonal wind and precipitation are negligible.

Key words: sea ice, Liaodong Bay, RCP scenarios, NEMO, LIM2

Citation: Guo Donglin, Li Rui, Zhao Peng. 2021. The long-term trend of Bohai Sea ice in different emission scenarios. Acta Oceanologica Sinica, 40(7): 100–118, doi: 10.1007/s13131-021-1703-8

1 Introduction

The Bohai Sea (Fig. 1) is a shallow marginal sea between 37.0°–41.0°N, 117.5°–121.5°E. It is largely enclosed by land with dense population and connected to the Yellow Sea via the Bohai Strait. The Bohai Sea includes three major bays, the Liaodong Bay (LDB) to the north, the Bohai Bay (BHB) to the west and the Laizhou Bay (LZB) to the south. Affected by cold air from the north, seasonal sea ice appears every winter, making the Bohai Sea one of the south most regions with sea ice in the Northern Hemisphere (Ning et al., 2009). Sea ice in the Bohai Sea usually appears in December and disappears in the following March, with a duration of 3–4 months.

Surrounded by dense populations, sea ice in the Bohai Sea is a great threat to local human activities. It may block harbors, damage ships and oil platforms, causing not only economic loss, but also injuries, or even deaths. Thus, understanding the physical processes controlling the onset and offset of the sea ice, developing an accurate sea ice forecast system, and evaluating the long-term trend of the sea ice, are critical for the management of the Bohai Sea and urgently needed. Previous studies regarding the sea ice in this region are mainly based on observations, especially remote sensing (Karvonen et al., 2017; Ning et al., 2009; Ouyang et al., 2019; Shi and Wang, 2012a, b; Su et al., 2019, 2012; Su and Wang, 2012; Yan et al., 2020, 2017; Yuan et al., 2018, 2012; Zhang et al., 2015). Some numerical models have also been developed and employed in related investigations (Chen et al., 2003; Ji et al., 2015; Yan et al., 2019; Zhang et al., 2019). However, most previous studies are about the sea ice in either current or historical climate conditions. With increasing CO_2 concentration in the atmosphere and rapidly changing climate, the sea ice in the future will probably be largely different from what it is currently or historically. Zu et al. (2016) investigated how sea ice in the Bohai Sea and the Yellow Sea will respond to changes of 2-m air temperature during 2015–2045 in different CO_2 emission scenarios. They found that the largest sea ice decrease appears in a middle CO_2 emission scenario (RCP 4.5) but not higher CO_2 emission scenarios (RCP6.0 and RCP 8.5). To the best of the authors' knowledge, this is the only pioneering study exploring the future of sea ice in the Bohai Sea. However, there are still many unknowns. For example, how will the change of atmospheric

Foundation item: The National Key R&D Program of China under contract No. 2019YFC1408403; the Outstanding Young Talents Funding Project of the Cultivation Project for High-level-innovation Talents in Science and Technology, Ministry of Natural Resources, under contract No. 12110600000018003923.

*Corresponding author, E-mail: zhaopeng@ncs.mnr.gov.cn

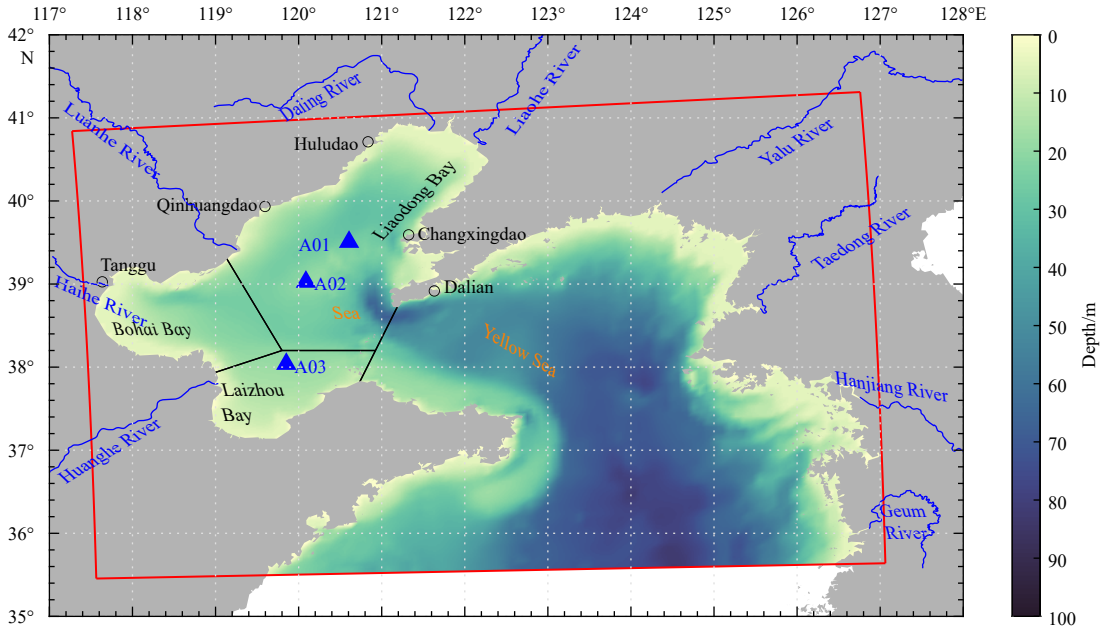

Fig. 1. Topography in the model domain. The edge of the domain is marked by the red lines. The blue lines indicate major rivers in this region, and the blue triangles indicate locations of buoys where sea surface temperature is measured.

factors other than 2-m temperature (e.g., downward shortwave radiation) influence the sea ice in the future? And how will the sea ice condition evolve with time after 2045?

Based on an ocean-sea ice coupled model, this study investigates the potential future of sea ice in the Bohai Sea from 2020 to 2100 in different CO_2 emission scenarios described by RCP 8.5, RCP 6.0, RCP 4.5 and RCP 2.6 (van Vuuren et al., 2011). The purpose of this study is to explore how the changing mean state of the atmosphere in the future may affect sea ice in the Bohai Sea, but not to forecast the sea ice condition at a specific instant. We first set up a control experiment in a typical winter with heavy sea ice, the winter of 2012–2013. A winter with heavy ice is selected intentionally since worst sea ice disasters mostly happen in such winters, especially in the future, in which a trend of weakening sea ice is expected with global warming. Influences from the changing atmospheric state will be evaluated by a set of sensitive experiments with updated mean state of the atmosphere according to predictions of climate models in different CO_2 emission scenarios.

Details of the experimental setup are described in Section 2. The results from the control experiment are compared with observations in Section 3. The future of sea ice in the Liaodong Bay is detailed in Section 4. The future of sea ice in the Bohai Bay and the Laizhou Bay is discussed in Section 5. The conclusions are summarized in Section 6.

2 Model setup

2.1 *Control experiment*

The Nucleus for European Modelling of the Ocean (NEMO; Madec et al., 2008) version 3.6 and Louvain-La-Neuve sea ice model 2 (LIM2; Fichefet and Maqueda, 1997; Goosse and Fichefet, 1999) are coupled to simulate sea ice in the Bohai Sea. The model domain covers the Bohai Sea and part of the Yellow Sea (Fig. 1), with an open boundary located south to the domain (~35.5°N). The model is based on a subset of the (1/12)° ORCA grid (Madec and Imbard, 1996). Its horizontal resolution is ~7.34 km in zonal direction and ~6.26 km in the meridional direction. In the vertical direction, a z-coordinate with 36 layers is adopted. The layer thickness is ~1 m near surface, increasing to ~4.4 m below 50 m. The topography is extracted from a 1-arcminute dataset, ETOPO1 (Amante and Eakins, 2009).

NEMO uses mode-splitting technology in time iteration. The time step for external mode and internal mode are 12 s and 360 s, respectively. The control experiment (Exp-Ctl) starts from April 1, 2012 and ends on April 30, 2013. Its initial fields, including temperature, salinity, current velocity and sea surface height, are extracted from (1/12)° HYCOM reanalysis Exp 53.x.

At surface, the net heat and freshwater flux are calculated on the fly by Core bulk formula (Large and Yeager, 2004). The hourly downward longwave radiation (DLR), downward shortwave radiation (DSR), 2-m air temperature, 2-m specific humidity, 10-m wind velocity and precipitation are extracted from the NCEP Climate Forecast System version 2 (NCEP CFSRv2; Saha et al., 2014). The surface forcing is given in river 0.2° grids except for precipitation, which is given in 0.5° grids.

At lateral boundaries, the partial slip condition is used for coastlines. Monthly climate freshwater runoff (Dai et al., 2009) from 8 major rivers (the Hanjiang River, the Liaohe River, the Geum River, the Yalu River, the Daling River, the Luanhe River, the Haihe River and the Taedong River) in the model domain is added as equivalent precipitation at the river mouths. At the open boundary located in the Yellow Sea, the model is forced by a combination of non-tidal components (temperature, salinity, current velocity and sea surface height extracted from 3-hourly HYCOM reanalysis Exp 53.x) and the tide-induced velocity/sea surface height from the Oregon State University's TPXO-08 dataset (Egbert and Erofeeva, 2002). Nine major tidal constituents in the Bohai Sea, including M_2, S_2, K_1, O_1, K_2, N_2, P_1, Q_1 and M_4, are considered in the model. The baroclinic component is relaxed to the pre-described values at the open boundary with a sponge layer of 10 grids. The barotropic signals are allowed to leave the domain freely with the Father radiation scheme (Flather, 1994).

The quadratic bottom drag is used in the model with a drag coefficient of 0.002 5. The Eddy-induced vertical mixing is parameterized by the generalized length scale (GLS) turbulent closure parameterization (Umlauf and Burchard, 2003, 2005).

2.2 *Sensitive experiments*

2.2.1 *Sensitive experiments for sea ice in the future*

A set of sensitive experiments (Exp-SE-a) is conducted to explore the wintertime sea ice in the Bohai Sea in the future with different CO_2 emission scenarios described by RCP 8.5, RCP 6.0, RCP 4.5 and RCP 2.6 (van Vuuren et al., 2011), in which the radiative forcing will increase to 8.5 W/m^2, 6.0 W/m^2, 4.5 W/m^2 and 2.6 W/m^2 in 2100, respectively. The mean states of the wintertime (November to March) atmosphere above the Bohai Sea in different scenarios (Fig. 2) are derived from the ensemble mean of climate models as listed in Table 1.

Due to the coarse spatial resolution of the climate models (~1.9° or above for atmosphere), they cannot capture the short- to medium-term atmospheric processes (e.g., cold air events) and the fine spatial distribution of the atmospheric variables above the Bohai Sea. Thus, changes of the mean state of wintertime atmosphere from the climate models are added to the atmospheric fields derived from NECP CFSRv2 to generate the surface forcing for the sensitive experiments. For each CO_2 emission scenario, the mean state of the wintertime atmosphere in 2012–2013 is first subtracted from that in a specific decade (e.g., 2021–2030), based on ensemble means of climate forecasts (Table 1); then the differences (Tables A1–A4) are added to the NCEP CFSRv2 hourly forecast for the winter of 2012–2013 to generate surface forcings for sensitive experiments. The wintertime surface forcings used in the sensitive experiments would be identical to the ones used in the control experiment after their mean values removed. Similar to the control experiment, each

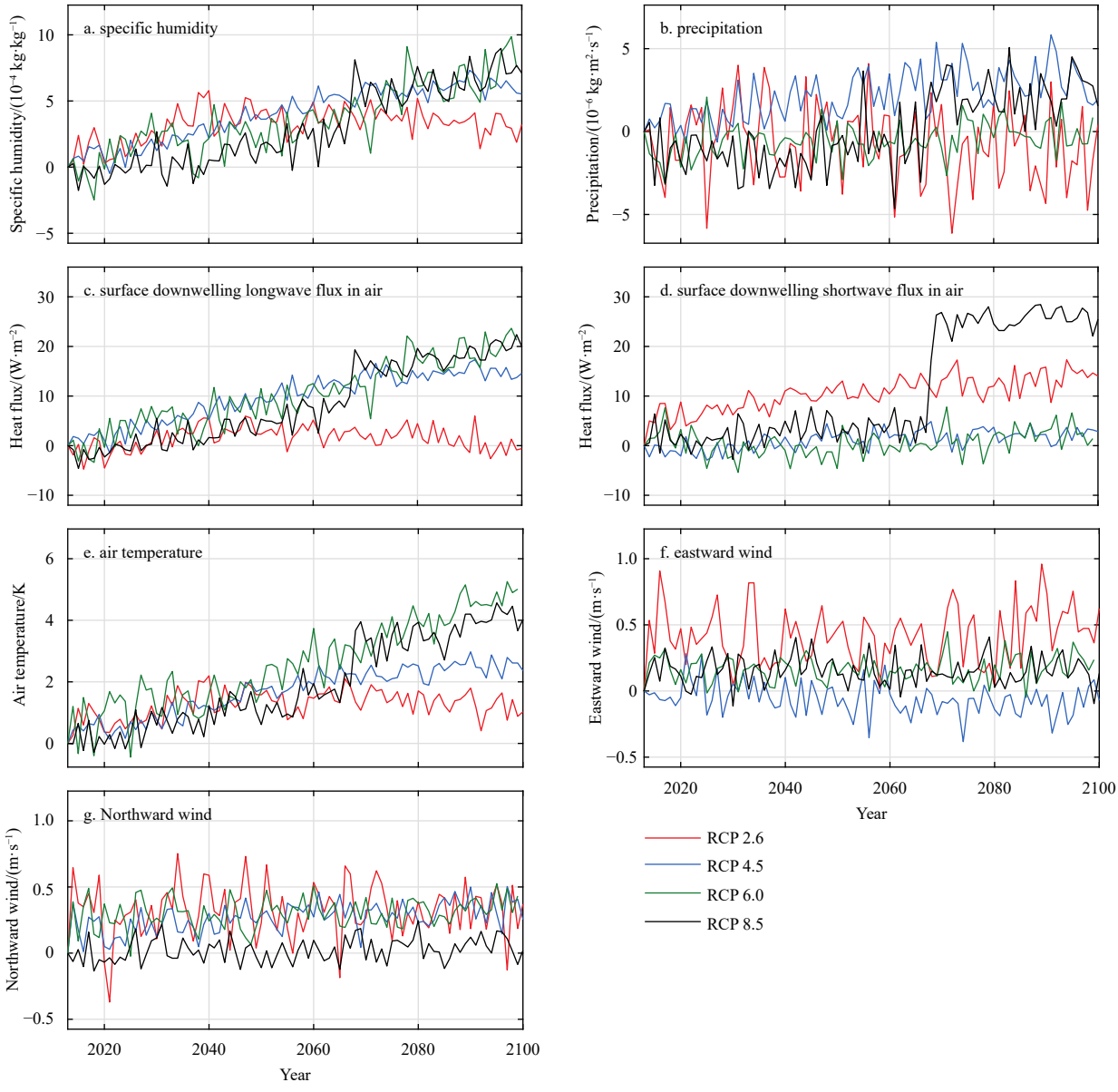

Fig. 2. Changes of wintertime (November to March) averaged 2-m specific humidity (a), precipitation (b), surface downward longwave radiation (c), surface downward shortwave radiation (d), 2-m air temperature (e), and 10-m wind in the zonal (f) and meridional (g) directions above the Bohai Sea in different CO_2 emission scenarios compared to the winter of 2012–2013.

Table 1. Sources of mean state of atmosphere in different CO_2 emission scenarios

Scenario	Model	Ensemble members	Reference
RCP 8.5	GFDL-GSM2M	r10i1p1–r19i1p1	Rodgers et al. (2015)
RCP 6.0	HadGEM2-ES	r1i1p1–r4i1p1	Collins et al. (2011)
RCP 4.5	CSIRO-MK3.6	r1i1p1–r10i1p1	Rotstayn et al. (2010)
RCP 2.6	CanESM2M	r1i1p1–r5i1p1	Arora et al. (2011)

sensitive experiment runs from April 1 to 30 in the next year. The above surface forcing for the sensitive experiments can, on one hand, reflect influences of changes in the mean state of the wintertime atmosphere, and on the other hand, keep the sensitive experiments comparable with the control experiment. The Bohai Sea is well mixed in winter (Bian et al., 2016), allowing the surface atmospheric forcings to influence the entire water column. The wintertime water temperature in the Bohai Sea is determined by the atmospheric forcing, while the initial temperature (in April) has little influence on it. Section A1 of Appendix shows that influences from the initial temperature and salinity fields in April can be ignored for wintertime sea ice. Thus, all sensitive experiments share the same initial fields with the control experiment.

2.2.2 *Sensitive experiments for different atmospheric variables*

Another set of sensitive experiments (Exp-SE-b) is used to further investigate the role of each atmospheric factor (e.g., air temperature) on future sea ice changes. Those experiments are similar to the ones described in Section 2.2.1, except that the mean value of only one of the atmospheric variables will be edited according to the climate forecasts in each experiment. The unchanged variables remain the same as in the control experiment. Thus, sea ice changes in each experiment in Exp-SE-b are exclusively caused by a specific atmospheric variable. Those experiments are only conducted for the 2090s.

3 Model validation

Accurate sea surface temperature (SST) is necessary for sea ice modelling. Figure A3 compares the modelled and observed daily SST (extracted from *in-situ* buoy observation) at three stations A01–A03 (triangles in Fig. 1). The highest SST (~25°C) appears in August and the lowest temperature (~0°C) appears in February. The control run is slightly biased from the observations from May to October and fails to reproduce the observed short-term perturbations in this period. However, the SST in control run matches the observations well after October, which includes the entire lifecycle of the sea ice in the Bohai Sea. Since the sea ice only appears in winter, the errors in summer will not affect the sea ice simulation investigated in this study.

Figure 3 compares the sea ice from the control experiment to true-color images from the Moderate Resolution Imaging Spectroradiometer (MODIS) carried by satellite Terra. It shows that the simulated sea ice extent (bounded by 15% contour of sea ice concentration) matches the MODIS images well, especially for

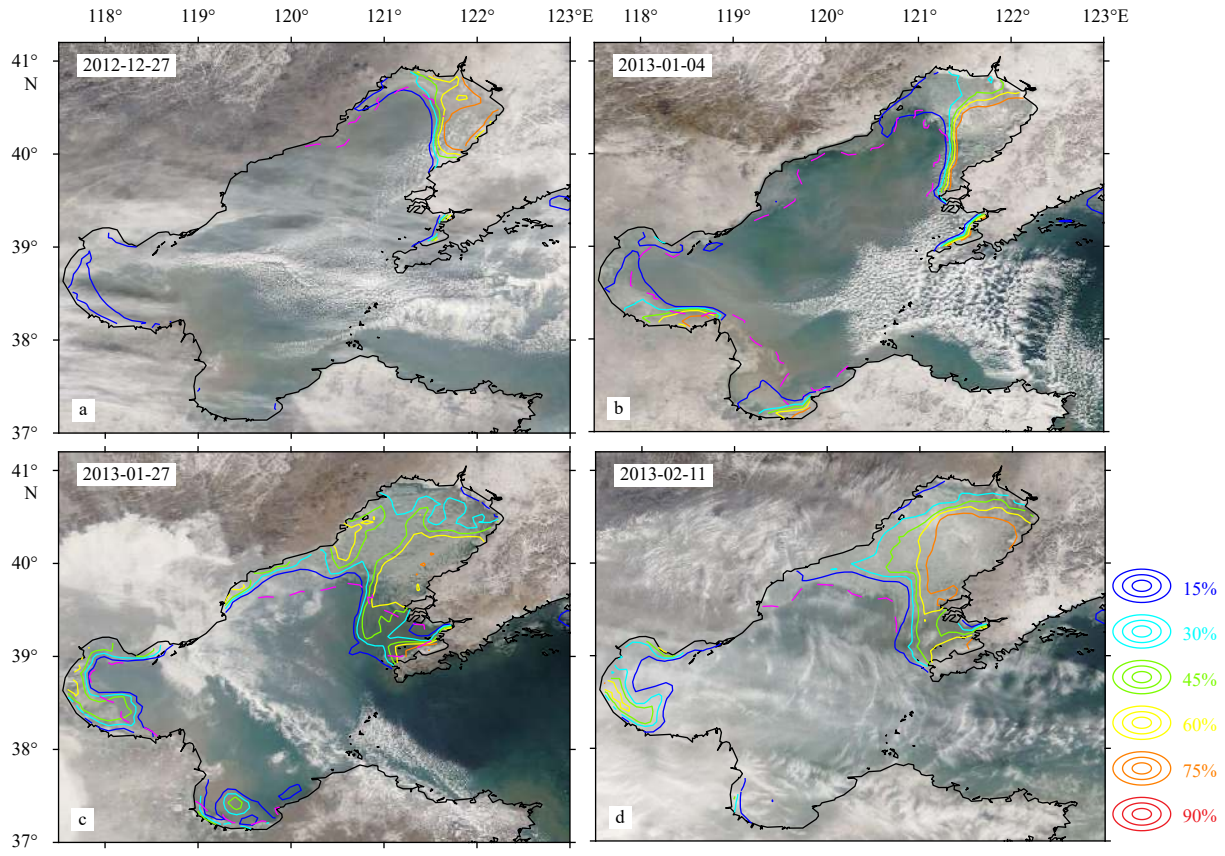

Fig. 3. True color images from MODIS (background image) and contours of sea ice concentration (solid colorful lines) from the control experiment. The dashed lines indicate sea ice extent subjectively derived from the satellite images.

the Liaodong Bay.

On December 27, 2012, the sea ice extent covered the north end of the Liaodong Bay with most of the sea ice appearing near the east side of the bay. The model indicates that sea ice also appeared in the Bohai Bay, which is hard to see in the satellite image due to clouds. On January 4 and 27, the Bohai Bay and the Laizhou Bay are relatively free of clouds. The simulated sea ice extent is consistent to the MODIS images in the Bohai Bay, while the model overestimates the area of sea ice extent in the Laizhou Bay. The Yellow River runs into the ocean at the west corner of the Laizhou Bay. In NEMO, river runoff is treated as equivalent precipitation in a region near the river mouth. The area of the region increases with the river runoff. This special way of adding river runoff may generate false distribution of salinity in the Laizhou Bay, which may contribute to the sea ice bias in the Laizhou Bay on January 4 and January 27. Since sea ice in the Bohai Sea mainly appears in the Liaodong Bay, small biases in the Laizhou Bay will not affect the major conclusions in this study. Around February 11, 2013, the area of sea ice extent in the Liaodong Bay reached its maxima in the winter of 2012–2013, covering almost the entire Liaodong Bay. Overall, the model can reproduce the observed sea ice distribution in the Bohai Sea well.

To evaluate the model results quantitively, Fig. 4 compares the daily area of the Bohai Sea where sea ice concentration is greater than 10% in the control experiment and the satellite-based sea ice analysis product provided by Japan Meteorological Agency. Only the days with less than 10% of cloud cover in the Bohai Sea are considered. The model results agree well with the analysis product, especially for the Liaodong Bay. The correlation coefficient between the two is 0.99 for the entire Bohai Sea, 0.96 for the Bohai Bay, 0.93 for the Laizhou Bay and 0.98 for the Liaodong Bay, all of which are significant at 99% level.

4 Sea ice in the Liaodong Bay

The onset and offset of sea ice in different scenarios share many similarities with largest changes in RCP 8.5. To keep the manuscript concise and avoid repeating similar results, the following discussions will first detail the sea ice in the RCP 8.5 scenario. Then, sea ice in the RCP 6.0, RCP 4.5 and RCP 2.6 scenarios will be introduced briefly, focusing on their differences from the RCP 8.5 scenario.

4.1 *RCP 8.5 scenario*

The most apparent feature in the RCP 8.5 scenario (black lines in Fig. 2) is probably the abrupt increase of downward shortwave radiation (hereafter DSR) around 2070, accompanied by a rapid change of specific humidity, downward longwave radiation (hereafter DLR) and 2-m air temperature. We checked the predicted DSR in the RCP 8.5 scenario in 14 different products. Similar abrupt changes appear in 10 of the 14 products. And the abrupt changes appear near 2070 in 8 of the 10 products. The reason for the abrupt change is interesting and worth further in-

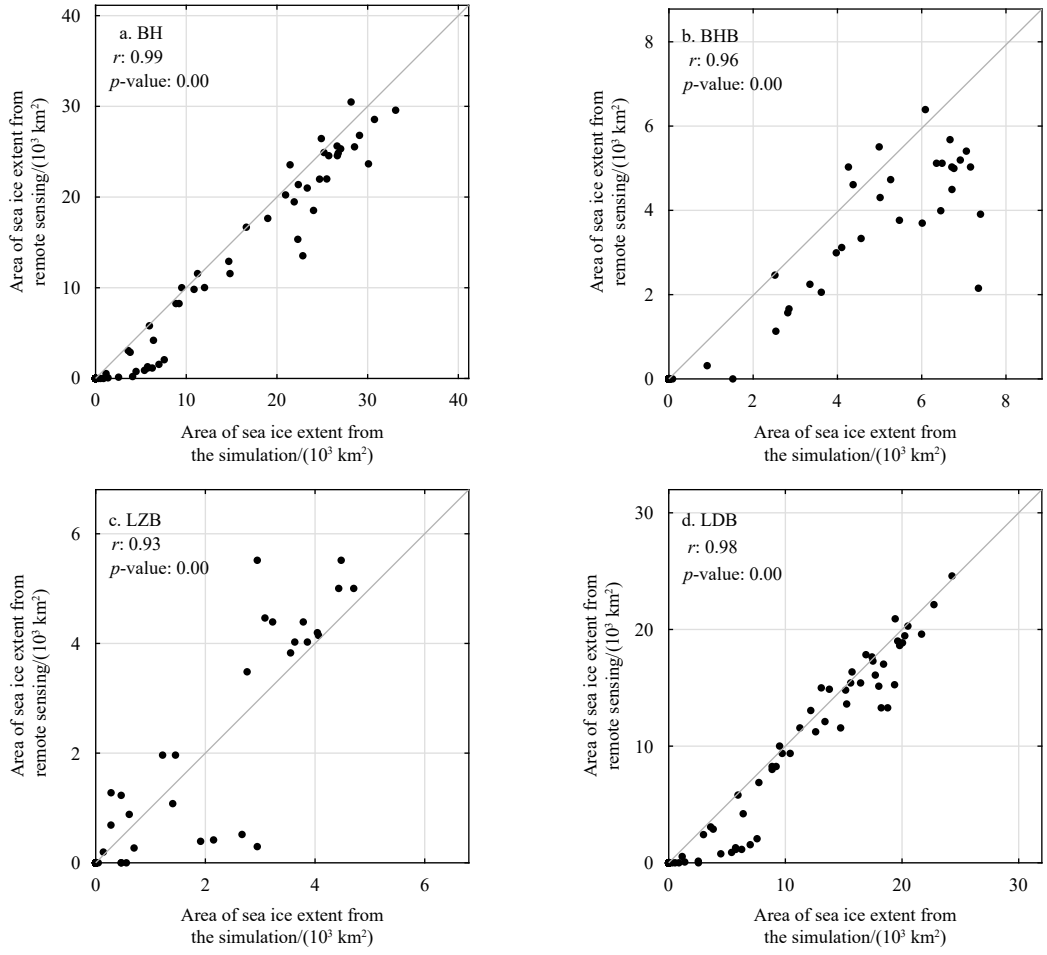

Fig. 4. Area of sea surface occupied by sea ice with a concentration of more than 10% from the control run (x axis) and remote sensing (y axis) in the Bohai Sea (BH, a), the Bohai Bay (BHB, b), the Laizhou Bay (LZB, c) and the Liaodong Bay (LDB, d). The correlation coefficient (r) and corresponding p-value are indicated at the upper-left corner of each panel.

vestigations. However, it is out the scope of this study.

A set of sensitive experiments, Exp-SE-a, for the future in the RCP 8.5 scenario suggest that the high CO_2 emissions will weaken the severity of wintertime sea ice in the Liaodong Bay. The results of those sensitive experiments are summarized in Figs 5–9 and Figs A4–A7. According to the sea-ice duration (Fig. 5a) and the maximum sea ice extent (Fig. 6a) in the Liaodong Bay, the remaining 80 years of this century, 2021–2100, can be divided into 3 periods: the mild decreasing period (2021–2060), the rapid decreasing period (2061–2080) and the decreasing period (2081–2100).

4.1.1 *The mild decreasing period (2021–2060)*

In 2021–2060, the severity of wintertime sea ice in the

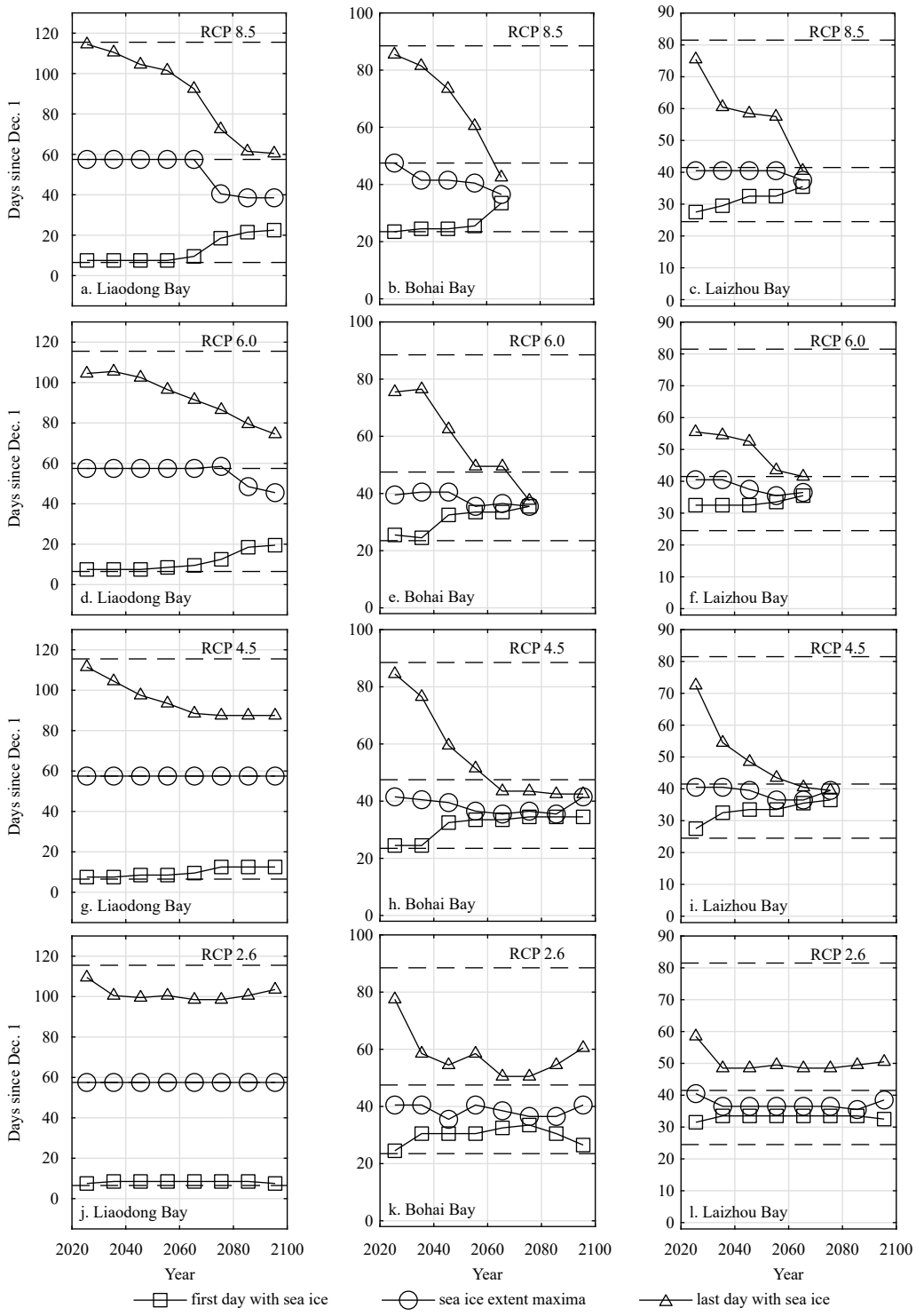

Fig. 5. The date of first ice, maximum sea ice extent and last ice in different CO_2 emission scenarios derived from sensitive experiments Exp-SE-a. The dashed horizontal lines indicate the corresponding values in the control experiment for the winter of 2012–2013.

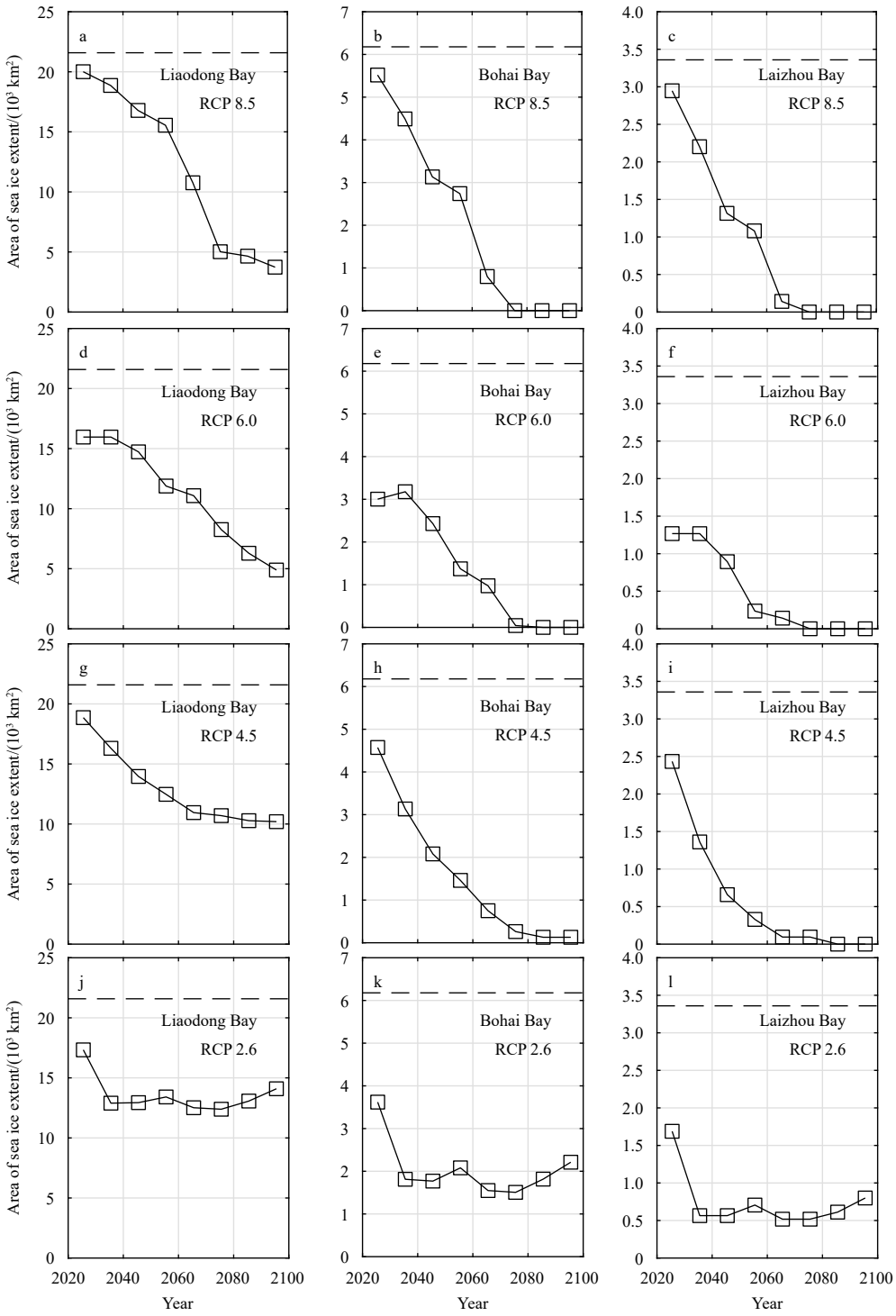

Fig. 6. The area of max sea ice extent in different CO_2 emission scenarios from sensitive experiments Exp-SE-a. The dashed horizontal lines indicate the corresponding values in the control experiment for the winter of 2012–2013.

Liaodong Bay will be weakening at a relatively mild and stable rate. The maximum sea ice extent will decrease ~150 km^2/a (Fig. 6a). The sea ice area and the total sea ice volume will also decrease compared to the winter of 2012–2013 from the first day with sea ice to the last day with sea ice in each winter (Figs 7 and 8). However, the mean thickness of the sea ice will be relatively stable (Fig. 9), especially in the first two decades (2021–2040). In the mild decreasing period, the date of last ice will arrive earlier, while the date of first ice and maximum sea ice extent, which are December 7 and January 27, respectively, will not be affected by the changes of the mean atmospheric state (Fig. 5a).

The weakening in the severity of sea ice is not uniform in the Liaodong Bay (Fig. A4). On the day with maximum sea ice extent area in each winter, the sea ice thickness and concentration decrease with time in the west side of the bay. While in the east side

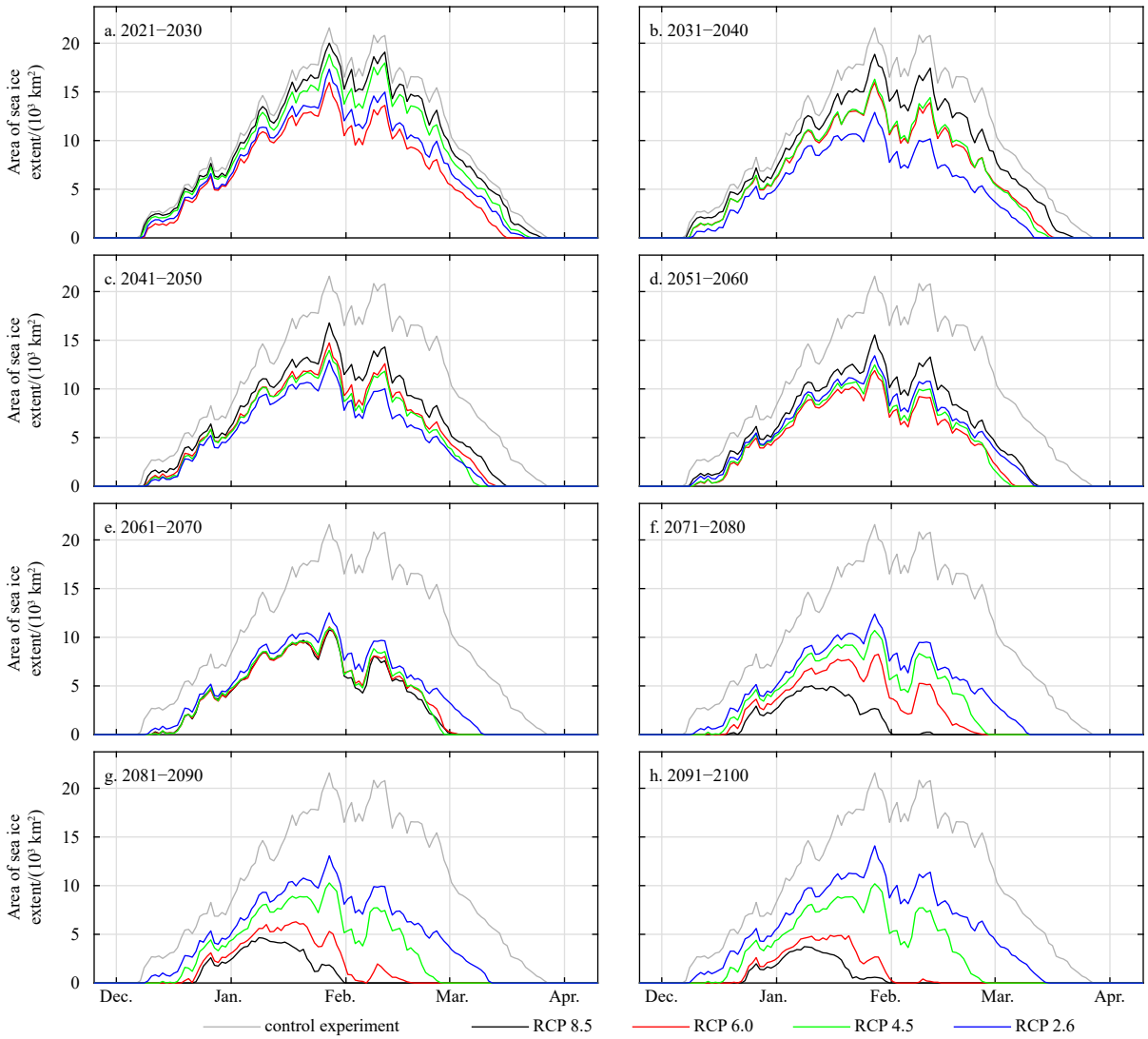

Fig. 7. Area of sea ice extent with a concentration of more than 15% in the Liaodong Bay from the control experiment and the sensitive experiments Exp-SE-a.

of the bay, the area of sea ice more than 20-cm thick is nearly unchanged. Only the area of sea ice exceeding 50 cm in thickness reduces significantly. Along the east coast of the bay, the sea ice maintains a concentration of ~70% with its thickness exceeding 40 cm. Overall, the severest sea ice condition will be relieved along the west coast of the bay, but not at the east coast of the bay.

4.1.2 *The rapid decreasing period (2061–2080)*

In this period, the maximum sea ice extent and the sea ice duration in the Liaodong Bay will decrease rapidly, from 16 000 km^2 and 95 d in 2051–2060 to 5 000 km^2 and 55 d in 2071–2080 (Fig. 5a). This is accompanied by the postponed first day with sea ice and a dramatic drop of mean sea ice thickness (Fig. 9). At the end of this period, only sparse sea ice can be found along the west coast of the bay, with a concentration of less than 15% and a thickness of less than 10 cm (Fig. A4). In the east side of the bay, the sea ice thickness reduces to below 30 cm, with a maximum sea ice concentration of ~60%.

Compared to 2021–2060, a significant difference in this rapid weakening period is the missing of the re-freezing process in February (Figs 7–9). Before 2061, the sea ice in the Liaodong Bay melts slightly near the end of January, and then refreezes quickly in early February. However, this refreezing process has disappeared since 2071–2080, with little sea ice remaining in February. This change is likely to be a result of rapid climate change around 2070, as shown in Fig. 2.

4.1.3 *The stabilized period (2081–2100)*

After 2080, the sea ice in the Liaodong Bay is relatively stable and much weakened compared to the winter of 2012–2013. The duration of sea ice is ~40 d and the maximum sea ice extent is ~5 000 km^2 (Figs 5a and 6a). Sea ice with a concentration of more than 15% can only be found in a small region near the north end and east coast of the bay (Fig. A4).

4.2 *The RCP 6.0, 4.5 and 2.6 scenarios*

Different from RCP 8.5, there is no abrupt change in the atmospheric states in the RCP 6.0, 4.5 and 2.6 scenarios (Fig. 2). In the RCP 6.0 scenario, the DLR and air temperature increase at a near-constant rate till the end of this century, by when the air temperature in RCP 6.0 is even higher than that in RCP 8.5. In the RCP 4.5 scenario, the DLR and air temperature increase at a rate

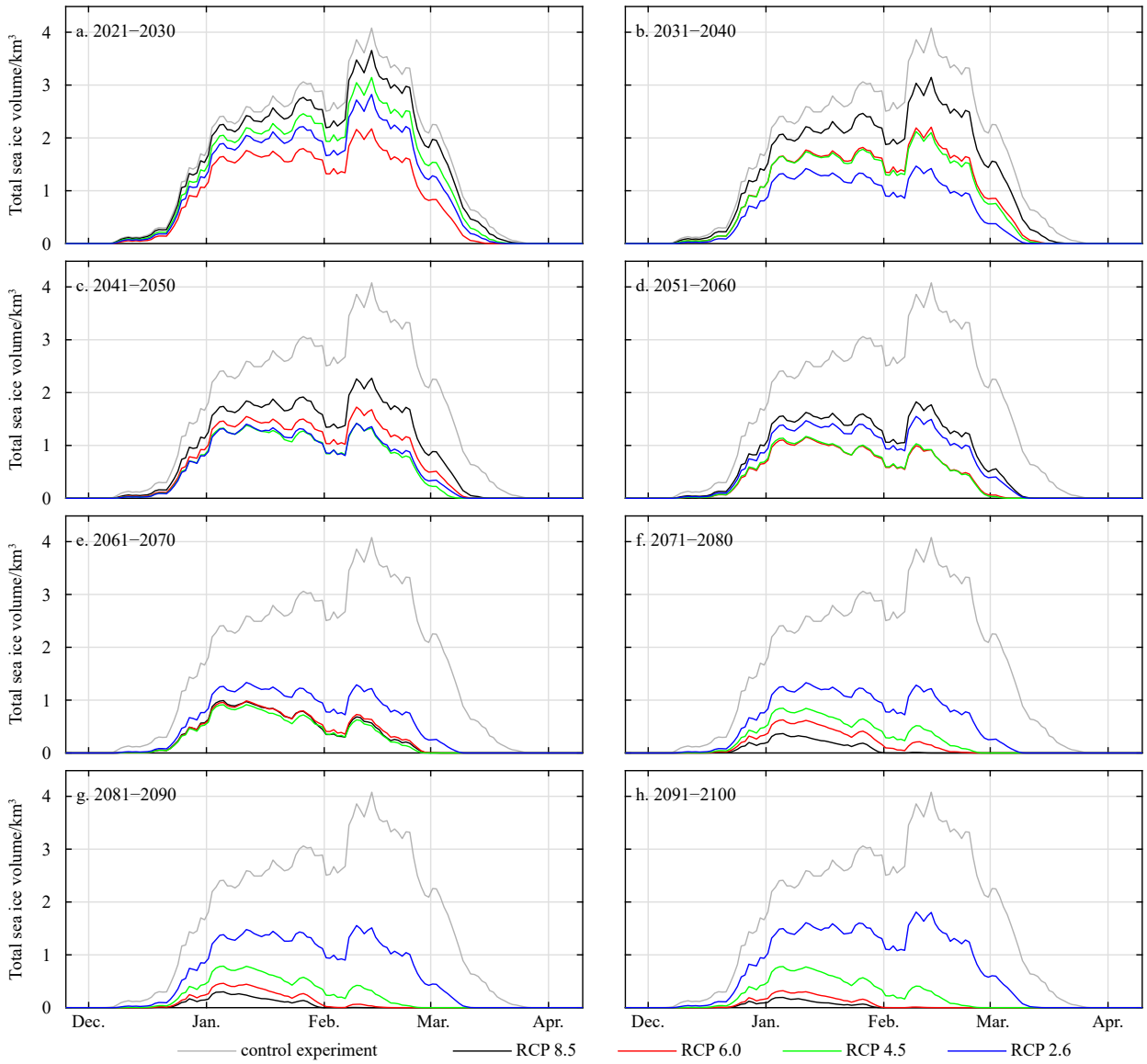

Fig. 8. Total volume of sea ice in the Liaodong Bay from the control experiment and the sensitive experiments Exp-SE-a.

similar to RCP 6.0 until they stabilize around 2070. In the RCP 2.6 scenario, DLR and air temperature increase (decrease) with time before 2040 (after 2080).

Not surprisingly, the similarities and differences of the atmosphere state in the four scenarios are reflected by the corresponding sea ice conditions, especially the date of last ice (Fig. 5) and the max sea ice extent area (Fig. 6). Starting with a descending trend, the max sea ice extent area keeps decreasing till the end of the century in RCP 6.0. In RCP 4.5, it stabilizes from around 2070. And in RCP 2.6, it stabilizes around 2040 but an increasing trend appears after 2080. Similar phenomena can also be found in the date of last ice among different scenarios.

The 2-D evolution of wintertime sea ice concentration and thickness in RCP 6.0, 4.5 and 2.6 is similar to that in RCP 8.5 as shown in Figs A4–A7 of the supplementary materials for readers' conveniences. To keep the manuscript clear and concise, the details will not be repeated here.

At the end of the 21st century, the sea ice in the Liaodong Bay will decrease most in RCP 8.5, less in RCP 6.0, less in RCP 4.5, and least in RCP 2.6. Compared to the winter of 2012–2013, the sea ice extent and volume of the Liaodong Bay in RCP 2.6 will largely decrease by the 2090s (Figs 7 and 8). While the mean sea ice thickness will only decrease slightly (Fig. 9) by then.

The above results are different from Zu et al. (2016), which suggested that the sea ice decreases most in the RCP 4.5 scenario. This difference is due to the different situations considered in Zu et al. (2016) and this study: (1) influences from all the atmospheric variables used to force the numerical model are considered in this study, while Zu et al. (2016) only investigated influences of 2-m air temperature; and (2) the results of Zu et al. (2016) are based on the mean air temperature of 2015–2045, which is before the abrupt change of the atmospheric state in the RCP 8.5 scenario. Figure 6 in this study also shows that the decrease of sea ice extent of the Liaodong Bay is larger in RCP 4.5 than RCP 8.5 in 2045.

4.3 *The role of each atmospheric variable*

To further investigate the role of each atmospheric variable on the sea ice decline in the Liaodong Bay, their contributions are evaluated in Fig. 10 by comparing differences between the control experiment and the two sets of sensitive experiments for

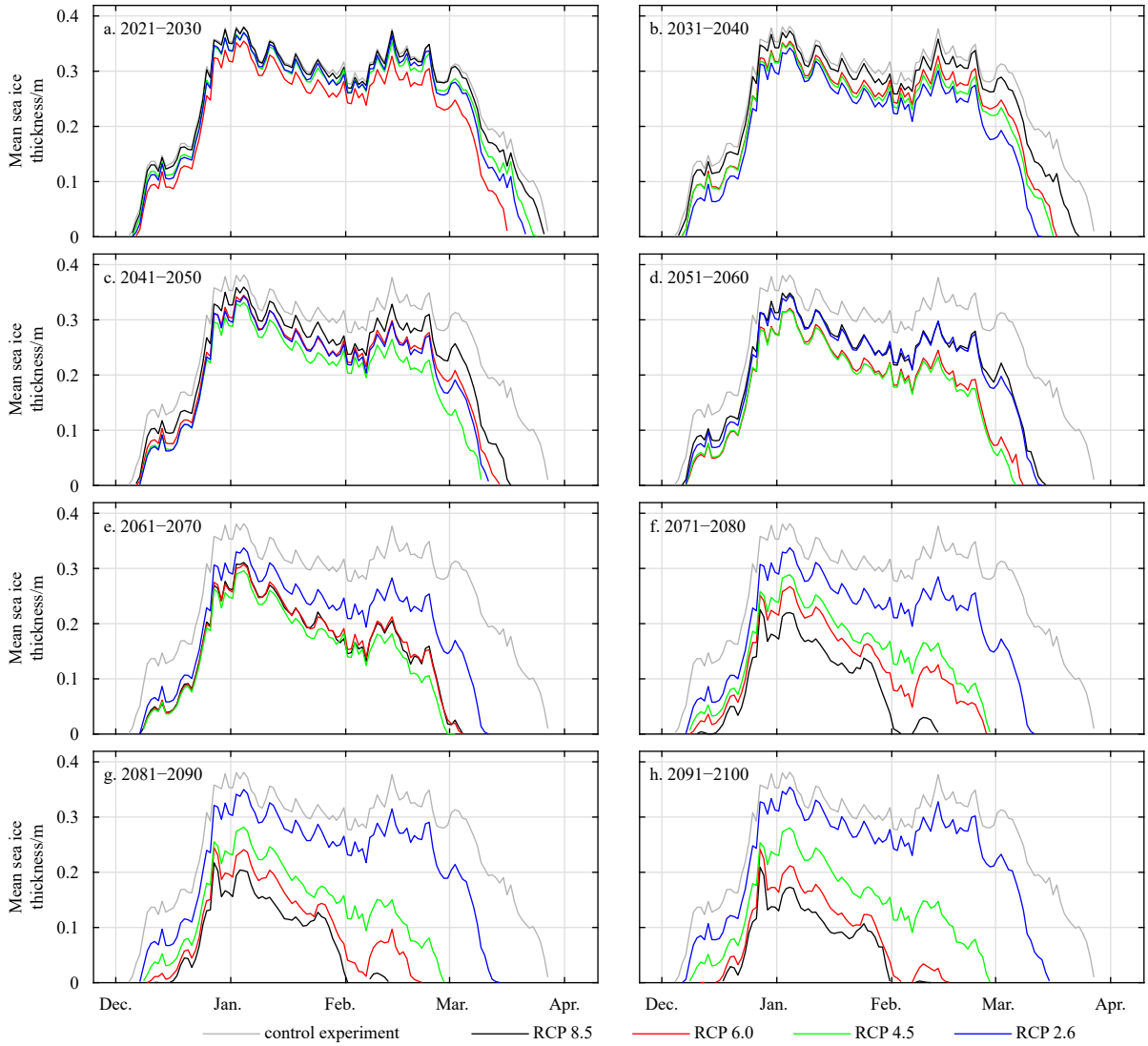

Fig. 9. Mean thickness of the sea ice in the Liaodong Bay from the control experiment and the sensitive experiments Exp-SE-a.

the 2090s, Exp-SE-a and Exp-SE-b. In the Exp-SE-a, the mean values of all atmospheric variables are edited following the climate forecasts, while, in the Exp-SE-b, only one of the atmospheric variables is edited in each run and the others remain unchanged from the control experiment. Thus, the first bar plot in each panel of Fig. 10 reflects the change of the sea ice extent due to the overall atmospheric state. And the remaining bar plots indicate the exclusive influences of the corresponding atmospheric variable on the change of the sea ice extent.

The results suggest that air temperature plays a leading role in the decline of the sea ice extent in the Liaodong Bay among the four CO_2 emission scenarios. Specific humidity also plays an important role in all the scenarios. DLR, DSR and meridional wind are important in certain scenarios when the changes of themselves are large. While influences from zonal wind and precipitation can be ignored. Those results also indicate that the sea ice extent decline to the end of the century in the Liaodong Bay is due to a combination of effects from multiple atmospheric factors. Even though air temperature is found to be the most important factor, none of the variables can dominate the magnitude of sea ice extent decline alone.

5 The Bohai Bay and the Laizhou Bay

5.1 *RCP 8.5 scenario*

Different from the Liaodong Bay, the state of sea ice in the Bohai Bay, including maximum sea ice extent area, mean sea ice thickness and total sea ice volume, weakens at a relatively stable rate. Its maximum sea ice extent decreases ~110 km^2/a. In 2021–2060, sea ice extent with a thickness of more than 10 cm still appears along the west and north coast of the bay during the sea ice maximum. The sea ice with a concentration of 15% or above disappears from the bay after 2071. And the Bohai Bay is completely free of sea ice after 2091. Between 2071–2090, only sparse sea ice less than 1 cm thick can be found. The date of first ice in the Bohai Bay is approximately unchanged until the 2060s, one decade before the disappearance of sea ice there.

Similar to the Bohai Bay, the state of sea ice in the Laizhou Bay weakens at a relatively stable rate. The maximum sea ice extent decreases ~70 km^2/a. The Laizhou Bay is completely free of sea ice after 2071.

5.2 *RCP 2.6, 4.5 and 6.0 scenarios*

For the Bohai Bay, the area of max sea ice extent in the RCP

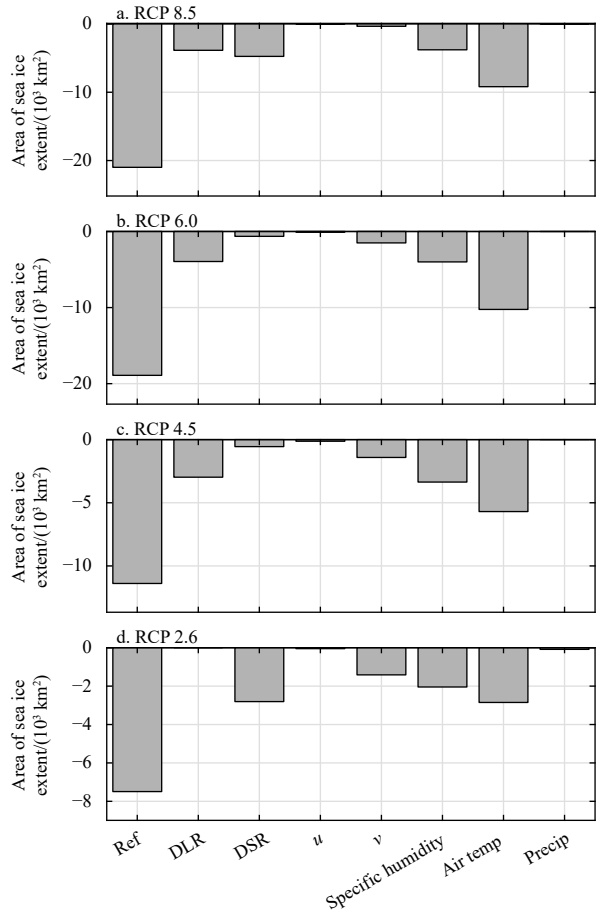

Fig. 10. The role of each atmospheric factor in the sea ice extent decline to the end of the 21st century. The first bar of each panel (noted as Ref) shows the difference between sea ice extent area on January 27 in the winter of the 2090s (from the sensitive experiments Exp-SE-a) and the winter of 2012–2013 (from the control experiment) in the Liaodong Bay. The other bars indicate the area differences between the control experiment and the sensitive experiments Exp-SE-b, in which only one of the atmospheric variables (noted in *x*-axis) is edited according to the climate forecasts for the 2090s and the others remain unchanged from the control experiment.

6.0 scenario keeps decreasing after the 2020s until the sea ice extent disappears in the 2070s (Fig. 6). In the RCP 4.5 scenario, it decreases from the 2020s to the 2080s, by when it stabilizes at ~128 km^2. In the RCP 2.6 scenario, it decreases to 1 812 km^2 in the 2030s, maintaining an area between 1 500 km^2 and 2 100 km^2 for several decades, until it starts to increase in the 2080s.

The evolution of max sea ice extent for the Laizhou Bay in the RCP 6.0, 4.5 and 2.6 scenarios is similar to that in the Bohai Bay, except that, in the RCP 4.5 scenario, the Laizhou Bay will be free of sea ice extent from the 2080s.

6 Discussion and conclusions

Using a coupled ocean-sea ice model based on NEMO 3.6 and LIM2, for the first time, this study investigates the potential future of sea ice in the Bohai Sea from 2020 to 2 100 in different CO_2 emission scenarios (RCP 8.5, 6.0, 4.5 and 2.6). The sea ice in a typical winter with heavy sea ice, the winter of 2012–2013, is first reproduced in the control experiment. Then, influences from the changing mean state of the atmosphere are evaluated by sensitive experiments.

The wintertime sea ice severity in the Bohai Sea weakens with time in the RCP 8.5 scenario. In the Liaodong Bay, the sea ice condition can be divided into 3 periods: the mild decreasing period (2021–2060), in which the sea ice severity weakens at a near-constant rate; the rapid decreasing period (2061–2080), in which the sea ice severity drops dramatically; and the stabilized period (2081–2100). At the end of the current century, the sea ice with a concentration of more than 15% will only appear near the north end and east coast of the bay and the duration of wintertime sea ice will shorten to ~40 d. The north and west coasts of the Liaodong Bay will be free of sea ice thicker than 10 cm. In the Bohai Bay and the Laizhou Bay, sea ice with a concentration of 15% or above disappears in the 2070s. The rapid decreasing period is due to an abrupt change of local atmospheric state in RCP 8.5. This reminds us that climate change does not necessarily come smoothly. And it is also an example of how an abrupt change in the local atmosphere affects the ocean.

Before the 2060s, the dates of first ice in all the three bays are approximately unchanged, which suggests that the onset of the sea ice is probably determined by a cold-air event and is not sensitive to the mean state of the atmosphere. It indicates that the accuracy of sea ice forecasts in the Bohai Sea largely depends on the accuracy of forecasts for cold air events. With decreasing sea ice severity, the mean and max sea ice thickness in the Liaodong Bay is relatively stable between 2021 and 2060 and then drops rapidly in the following 10 years.

In the RCP 6.0 scenario, the sea ice severity in the Bohai Sea weakens with time to the end of the current century. The Bohai Bay will be free of sea ice extent from the 2080s and the Laizhou Bay will be free of sea ice extent from the 2070s. In the RCP 4.5 scenario, the sea ice severity in the Bohai Sea weakens with time until it stabilizes in the 2070s. The Laizhou Bay will be free of sea ice extent from the 2080s. In the RCP 2.6 scenario, the sea ice severity will keep weakening before it stabilizes in the 2040s. After four decades in a stable state, it starts intensifying after the 2080s. Sea ice extent will appear in all the three bays of the Bohai Sea in the 2090s in this scenario.

Till the end of this century, sea ice in the Bohai Sea will decrease most in the RCP 8.5 scenario, less in the RCP 6.0 scenario, less in the RCP 4.5 scenario and least in the RCP 2.6 scenario.

Another set of sensitive experiments (Exp-SE-b) suggests that air temperature and specific humidity play important roles in the sea ice extent decline in the four scenarios. The surface downward shortwave/longwave radiation and meridional wind also matter in certain scenarios, while effects from the zonal wind and precipitation are negligible. Among all the atmospheric factors, air temperature is the leading factor in all scenarios, demonstrating the potentially huge impact of global warming on marginal seas and the importance of predicting the long-term trend of air temperature.

To fully understand the potential future of sea ice in the Bohai Sea, more winter conditions (e.g., choosing a different winter for the control experiment) should be discussed in future studies. Limited by the capacity of the climate projection models, only changes in the mean state of the atmosphere are considered in this study. However, the changes in the mean state of the atmosphere will affect the frequency and strength of short- to medium-term atmospheric processes, like cold air events. How the local atmospheric processes above the Bohai Sea will change in different scenarios and their two-way interactions with local sea ice also require further investigations.

Acknowledgements

The NCEP CFSRv2 product used in this study was downloaded from the Research Data Archive (https://rda.ucar.edu/). The HYCOM reanalysis Exp 53.X used in this study was downloaded from https://www.hycom.org/data/glbv0pt08/expt-53ptx. The GFDL-ESM2M simulation in the RCP 8.5 scenario is available from https://www.earthsystemgrid.org/dataset/ucar.cgd.ccsm4.CLIVAR_LE.gfdl_esm2m_lens.html. The other HadGEM2-ES simulation for RCP 6.0, the CSIRO-MK3.6 simulation for RCP 4.5 and the CanESM2M simulation for RCP 2.6 are available from https://cds.climate.copernicus.eu/cdsapp#!/home. The true color images of the earth surface from MODIS are available from the Earth Data website by NOAA (https://earthdata.nasa.gov/). Daily analyses of sea ice concentration are available from the Japan Meteorological Agency (https://ds.data.jma.go.jp/gmd/goos/data/pub/JMA-product/man_ice_okh_D/).

References

Amante C, Eakins B W. 2009. ETOPO1 1 arc-minute global relief model: procedures, data sources and analysis. NOAA Technical Memorandum NESDIS NGDC-24. Bouder, Colorado, USA: National Centers for Environmental Information, NOAA, https://www.ncei.noaa.gov/access/metadata/landing-page/bin/iso?id=gov.noaa.ngdc.mgg.dem:316

Arora V K, Scinocca J F, Boer G J, et al. 2011. Carbon emission limits required to satisfy future representative concentration pathways of greenhouse gases. Geophysical Research Letters, 38(5): L05805, doi: 10.1029/2010GL046270

Bian Changwei, Jiang Wensheng, Pohlmann T, et al. 2016. Hydrography-physical description of the Bohai Sea. Journal of Coastal Research, 74(10074): 1–12, doi: 10.2112/SI74-001.1

Chen Changsheng, Liu Hedong, Beardsley R C. 2003. An unstructured grid, finite-volume, three-dimensional, primitive equations ocean model: application to coastal ocean and estuaries. Journal of Atmospheric and Oceanic Technology, 20(1): 159–186, doi: 10.1175/1520-0426(2003)020<0159:AUGFVT>2.0.CO;2

Collins W J, Bellouin N, Doutriaux-Boucher M, et al. 2011. Development and evaluation of an Earth-System model–HadGEM2. Geoscientific Model Development, 4(4): 1051–1075, doi: 10.5194/gmd-4-1051-2011

Dai Aiguo, Qian Taotao, Trenberth K E, et al. 2009. Changes in continental freshwater discharge from 1948 to 2004. Journal of Climate, 22(10): 2773–2792, doi: 10.1175/2008JCLI2592.1

Egbert G D, Erofeeva S Y. 2002. Efficient inverse modeling of barotropic ocean tides. Journal of Atmospheric and Oceanic Technology, 19(2): 183–204, doi: 10.1175/1520-0426(2002)019<0183:EIMOBO>2.0.CO;2

Fichefet T, Maqueda M A M. 1997. Sensitivity of a global sea ice model to the treatment of ice thermodynamics and dynamics. Journal of Geophysical Research: Oceans, 102(C6): 12609–12646, doi: 10.1029/97JC00480

Flather R A. 1994. A storm surge prediction model for the northern bay of Bengal with application to the cyclone disaster in April 1991. Journal of Physical Oceanography, 24(1): 172–190, doi: 10.1175/1520-0485(1994)024<0172:ASSPMF>2.0.CO;2

Goosse H, Fichefet T. 1999. Importance of ice-ocean interactions for the global ocean circulation: a model study. Journal of Geophysical Research: Oceans, 104(C10): 23337–23355, doi: 10.1029/1999JC900215

Ji Qiyan, Zhu Xueming, Wang Hui, et al. 2015. Assimilating operational SST and sea ice analysis data into an operational circulation model for the coastal seas of China. Acta Oceanologica Sinica, 34(7): 54–64, doi: 10.1007/s13131-015-0691-y

Karvonen J, Shi Lijian, Cheng Bin, et al. 2017. Bohai sea ice parameter estimation based on thermodynamic ice model and earth observation data. Remote Sensing, 9(3): 234, doi: 10.3390/rs9030234

Large W G, Yeager S G. 2004. Diurnal to Decadal Global Forcing for Ocean and Sea-Ice Models: The Data Sets and Flux Climatologies. NCAR/TN-460+STR. Boulder, Colorado: National Center for Atmospheric Research, doi: 10.5065/D6KK98Q6, https://opensky.ucar.edu/islandora/object/technotes:434

Madec G, Imbard M. 1996. A global ocean mesh to overcome the North Pole singularity. Climate Dynamics, 12(6): 381–388, doi: 10.1007/BF00211684

Madec G, Bourdallé-Badie R, Bouttier P A, et al. 2008. NEMO ocean engine. Zenodo: Notes du Pôle de modélisation de l'Institut Pierre-Simon Laplace (IPSL), https://doi.org/10.5281/zenodo.3248739

Ning Li, Xie Feng, Gu Wei, et al. 2009. Using remote sensing to estimate sea ice thickness in the Bohai Sea, China based on ice type. International Journal of Remote Sensing, 30(17): 4539–4552, doi: 10.1080/01431160802592542

Ouyang Lunxi, Hui Fengming, Zhu Lixian, et al. 2019. The spatiotemporal patterns of sea ice in the Bohai Sea during the winter seasons of 2000–2016. International Journal of Digital Earth, 12(8): 893–909, doi: 10.1080/17538947.2017.1365957

Rodgers K B, Lin J, Frölicher T L. 2015. Emergence of multiple ocean ecosystem drivers in a large ensemble suite with an Earth system model. Biogeosciences, 12(11): 3301–3320, doi: 10.5194/bg-12-3301-2015

Rotstayn L D, Collier M A, Dix M R, et al. 2010. Improved simulation of Australian climate and ENSO-related rainfall variability in a global climate model with an interactive aerosol treatment. International Journal of Climatology, 30(7): 1067–1088, doi: 10.1002/joc.1952

Saha S, Moorthi S, Wu Xingren, et al. 2014. The NCEP climate forecast system version 2. Journal of Climate, 27(6): 2185–2208, doi: 10.1175/JCLI-D-12-00823.1

Shi Wei, Wang Menghua. 2012a. Sea ice properties in the Bohai Sea measured by MODIS-Aqua: 1. Satellite algorithm development. Journal of Marine Systems, 95: 32–40, doi: 10.1016/j.jmarsys.2012.01.012

Shi Wei, Wang Menghua. 2012b. Sea ice properties in the Bohai Sea measured by MODIS-Aqua: 2. Study of sea ice seasonal and interannual variability. Journal of Marine Systems, 95: 41–49, doi: 10.1016/j.jmarsys.2012.01.010

Su Hua, Ji Bowen, Wang Yunpeng. 2019. Sea ice extent detection in the Bohai Sea using sentinel-3 OLCI data. Remote Sensing, 11(20): 2436, doi: 10.3390/rs11202436

Su Hua, Wang Yunpeng. 2012. Using MODIS data to estimate sea ice thickness in the Bohai Sea (China) in the 2009–2010 winter. Journal of Geophysical Research: Oceans, 117(C10): C10018, doi: 10.1029/2012JC008251

Su Hua, Wang Yunpeng, Yang Jingxue. 2012. Monitoring the spatiotemporal evolution of sea ice in the Bohai Sea in the 2009-2010 winter combining MODIS and meteorological data. Estuaries and Coasts, 35(1): 281–291, doi: 10.1007/s12237-011-9425-3

Umlauf L, Burchard H. 2003. A generic length-scale equation for geophysical turbulence models. Journal of Marine Research, 61(2): 235–265, doi: 10.1357/002224003322005087

Umlauf L, Burchard H. 2005. Second-order turbulence closure models for geophysical boundary layers. A review of recent work. Continental Shelf Research, 25(7–8): 795–827, doi: 10.1016/j.csr.2004.08.004

van Vuuren D P, Edmonds J, Kainuma M, et al. 2011. The representative concentration pathways: an overview. Climatic Change, 109: 5, doi: 10.1007/s10584-011-0148-z

Yan Yu, Gu Wei, Xu Yingjun, et al. 2019. The *in situ* observation of modelled sea ice drift characteristics in the Bohai Sea. Acta Oceanologica Sinica, 38(3): 17–25, doi: 10.1007/s13131-019-1395-5

Yan Yu, Shao Dongdong, Gu Wei, et al. 2017. Multidecadal anomalies of Bohai Sea ice cover and potential climate driving factors during 1988–2015. Environmental Research Letters, 12(9): 094014, doi: 10.1088/1748-9326/aa8116

Yan Yu, Uotila P, Huang Kaiyue, et al. 2020. Variability of sea ice area in the Bohai Sea from 1958 to 2015. Science of the Total Environment, 709: 136164, doi: 10.1016/j.scitotenv.2019.136164

Yuan Shuai, Gu Wei, Xu Yingjun, et al. 2012. The estimate of sea ice resources quantity in the Bohai Sea based on NOAA/AVHRR data. Acta Oceanologica Sinica, 31(1): 33–40, doi: 10.1007/s13131-012-0173-4

Yuan Shuai, Liu Chengyu, Liu Xueqin. 2018. Practical model of sea ice thickness of Bohai Sea based on MODIS data. Chinese Geographical Science, 28(5): 863–872, doi: 10.1007/s11769-018-0986-y

Zhang Na, Wang Jin, Wu Yongsheng, et al. 2019. A modelling study of ice effect on tidal damping in the Bohai Sea. Ocean Engineering, 173: 748–760, doi: 10.1016/j.oceaneng.2019.01.049

Zhang Na, Wu Yongsheng, Zhang Qinghe. 2015. Detection of sea ice in sediment laden water using MODIS in the Bohai Sea: a CART decision tree method. International Journal of Remote Sensing, 36(6): 1661–1674, doi: 10.1080/01431161.2015.1015658

Zu Ziqing, Ling Tiejun, Zhang Yunfei, et al. 2016. Future projection of the sea ice in the Bohai Sea and the North Yellow Sea. Marine Forecasts (in Chinese), 33(5): 1–8

Appendix

A1 Sensitive to the initial fields

The following two additional sensitive experiments are conducted to explore how changes of the initial temperature and salinity fields in April may affect the wintertime sea surface temperature (SST), sea surface salinity (SSS) and sea ice: (1) Exp-Ini-Temp: it is identical to the control experiment except that 2°C is added to the 3-d initial temperature field; and (2) Exp-Ini-Salt: it is identical to the control experiment except that 1 g/kg is subtracted from the 3-d initial salinity field.

Figures A1a, c and e suggest that the effect of the increased initial temperature is suppressed quickly by surface forcing. The differences in SST between Exp-Ini-Temp and the control experiment are negligible from July. Since the Bohai Sea is well mixed in winter with near-vertical isotherms, this also indicates that the differences in the wintertime water temperature below sea surface are negligible. Thus, it is expected that the 2°C increase in the initial temperature has little influence on the sea ice simulation, which is proven by Figs A2a, c and e.

Different from Exp-Ini-Temp, the 1 g/kg decrease in the initial salinity field of Exp-Ini-Salt can last throughout the modelling period (Figs A1b, d and f). However, Figs A2b, d and f suggests that the change in the salinity field will not affect the sea ice in the Liaodong Bay significantly. The sea ice condition in the Bohai Bay and the Laizhou Bay is also examined, with no significant changes found (figures not shown).

Overall, for the wintertime seasice simulations conducted in this study, the effect from changes in initial temperature and salinity fields (in April) within a reasonable magnitude is negligible.

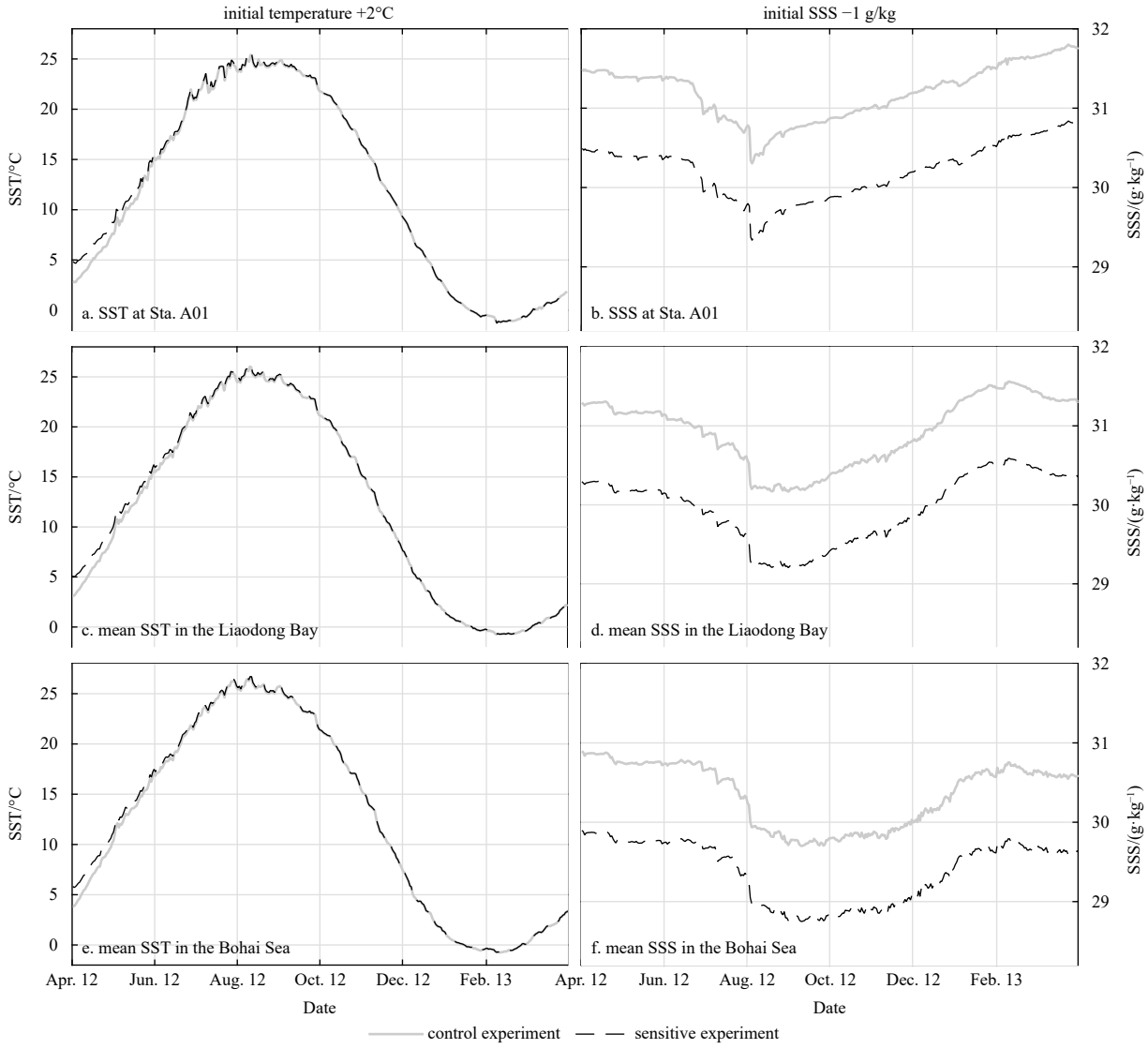

Fig. A1. Sea surface temperature (SST, a, c, e) from the control experiment (solid grey lines) and the sensitive experiment Exp-Ini-Temp (dashed black lines), whose initial temperature is 2°C higher than the control experiment; sea surface salinity (SSS, b, d, f) from the control experiment (solid grey lines) and the sensitive experiment Exp-Ini-Salt (dashed black lines), whose initial salinity is 1 g/kg lower than the control experiment. The location of station A01 is shown in Fig. 1.

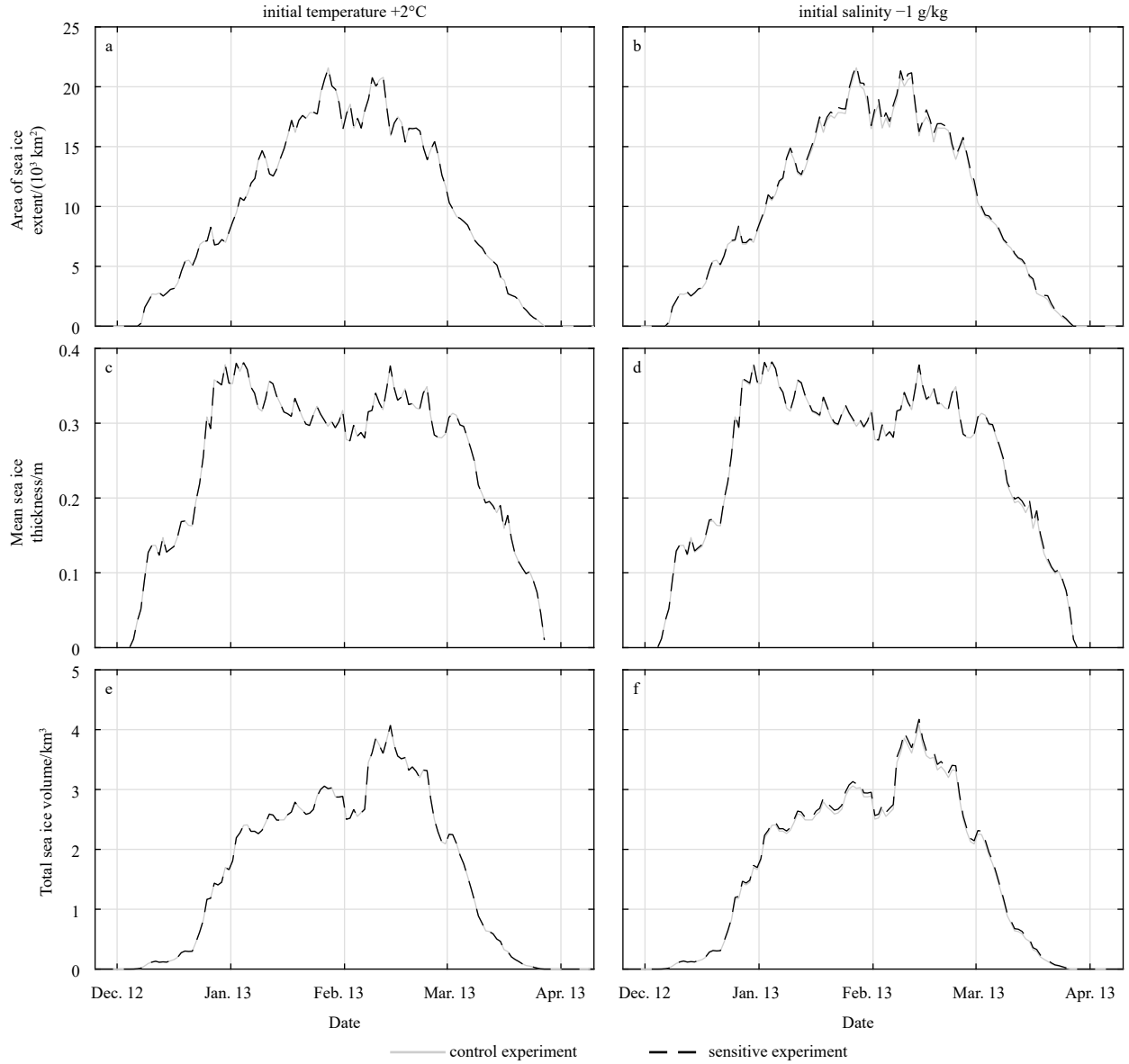

Fig. A2. Area of sea ice (a, b), Mean sea ice thickness (c, d), and total sea ice volume (e, f) from the control experiment (solid grey lines) and two sensitive experiments (dashed black lines), Exp-Ini-Temp (left panels), whose initial temperature is 2°C higher than the control experiment, and Exp-Ini-Salt (right panels), whose initial salinity is 1 g/kg lower than the control experiment.

A2 Tables and figures

Table A1. Change in wintertime (November to March) atmospheric conditions in the RCP 8.5 scenario compared to the winter of 2012–2013

Period	Specific humidity/ (10^{-6} kg·kg^{-1})	Precip/ (10^{-6} kg·m^{-2}·s^{-1})	DLW/ (W·m^{-2})	DSW/ (W·m^{-2})	Air temperature/°C	Zonal wind speed/(m·s^{-1})	Meridional wind speed/(m·s^{-1})
2021–2030	25.778	–1.168	0.419	0.664	0.366	0.121	0.011
2031–2040	–4.295	–2.028	0.934	2.967	0.744	0.160	0.028
2041–2050	126.452	–1.443	3.601	3.965	1.169	0.221	0.010
2051–2060	196.402	–0.406	6.185	3.297	1.368	0.112	0.002
2061–2070	357.875	0.146	10.523	9.757	2.285	0.147	0.033
2071–2080	568.938	2.331	15.989	25.236	3.349	0.170	0.062
2081–2090	628.251	2.028	17.717	25.554	3.550	0.140	0.016
2091–2100	723.334	2.475	19.798	25.913	4.098	0.151	0.067

Note: DSW and DLW indicate the surface downward shortwave radiation and the surface downward longwave radiation, respectively.

Table A2. Change in wintertime (November to March) atmospheric conditions in the RCP 6.0 scenario compared to the winter of 2012–2013

Period	Specific humidity/ (10^{-6} kg·kg^{-1})	Precip/ (10^{-6} kg·m^{-2}·s^{-1})	DLW/ (W·m^{-2})	DSW (W·m^{-2})	Air temperature/°C	Zonal wind speed/(m·s^{-1})	Meridional wind speed/(m·s^{-1})
2021–2030	204.237	–0.615	4.648	–0.407	1.339	0.164	0.277
2031–2040	170.118	–0.646	4.697	–0.736	1.373	0.134	0.301
2041–2050	263.688	–0.378	7.890	–1.925	1.680	0.152	0.245
2051–2060	289.583	–0.893	9.195	0.508	2.628	0.157	0.356
2061–2070	386.868	–0.545	11.638	0.213	2.846	0.163	0.304
2071–2080	548.500	–0.141	15.669	0.965	3.665	0.135	0.292
2081–2090	634.748	0.023	17.757	2.326	4.189	0.185	0.309
2091–2100	740.741	–0.137	19.990	2.700	4.737	0.232	0.385

Note: DSW and DLW indicate the surface downward shortwave radiation and the surface downward longwave radiation, respectively.

Table A3. Change in wintertime (November to March) atmospheric conditions in the RCP 4.5 scenario compared to the winter of 2012–2013

Period	Specific humidity/ (10^{-6} kg·kg^{-1})	Precip/ (10^{-6} kg·m^{-2}·s^{-1})	DLW/ (W·m^{-2})	DSW (W·m^{-2})	Air temperature/°C	Zonal wind speed/(m·s^{-1})	Meridional wind speed/(m·s^{-1})
2021–2030	102.536	0.655	2.829	–0.935	0.542	0.033	0.158
2031–2040	234.775	1.504	5.913	0.315	1.020	–0.003	0.221
2041–2050	344.460	1.941	8.611	1.225	1.504	–0.059	0.262
2051–2060	431.652	2.538	10.616	1.740	1.817	–0.045	0.289
2061–2070	539.022	2.861	12.811	2.294	2.227	–0.111	0.304
2071–2080	580.075	2.924	14.104	2.051	2.331	–0.105	0.307
2081–2090	617.175	3.163	14.758	2.141	2.454	–0.087	0.350
2091–2100	613.910	3.163	14.867	2.167	2.488	–0.098	0.329

Note: DSW and DLW indicate the surface downward shortwave radiation and the surface downward longwave radiation, respectively.

Table A4. Change in wintertime (November to March) atmospheric conditions in the RCP 2.6 scenario compared to the winter of 2012–2013

Period	Specific humidity/ (10^{-6} kg·kg^{-1})	Precip/ (10^{-6} kg·m^{-2}·s^{-1})	DLW/ (W·m^{-2})	DSW (W·m^{-2})	Air temperature/°C	Zonal wind speed/(m·s^{-1})	Meridional wind speed/(m·s^{-1})
2021–2030	169.520	0.049	–0.221	6.450	0.729	0.379	0.189
2031–2040	395.981	0.077	3.033	8.581	1.517	0.381	0.420
2041–2050	385.460	–0.017	2.982	10.611	1.488	0.416	0.329
2051–2060	350.707	–0.013	2.875	10.532	1.276	0.333	0.308
2061–2070	387.610	–1.115	2.174	12.442	1.564	0.358	0.332
2071–2080	399.049	–1.762	2.424	12.674	1.526	0.385	0.352
2081–2090	350.722	–1.659	1.158	13.290	1.395	0.559	0.314
2091–2100	300.425	–1.071	–0.015	13.855	1.098	0.510	0.327

Note: DSW and DLW indicate the surface downward shortwave radiation and the surface downward longwave radiation, respectively.

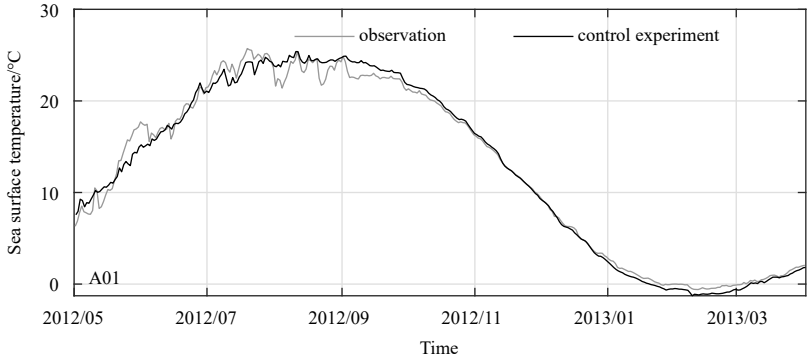

Fig. A3.

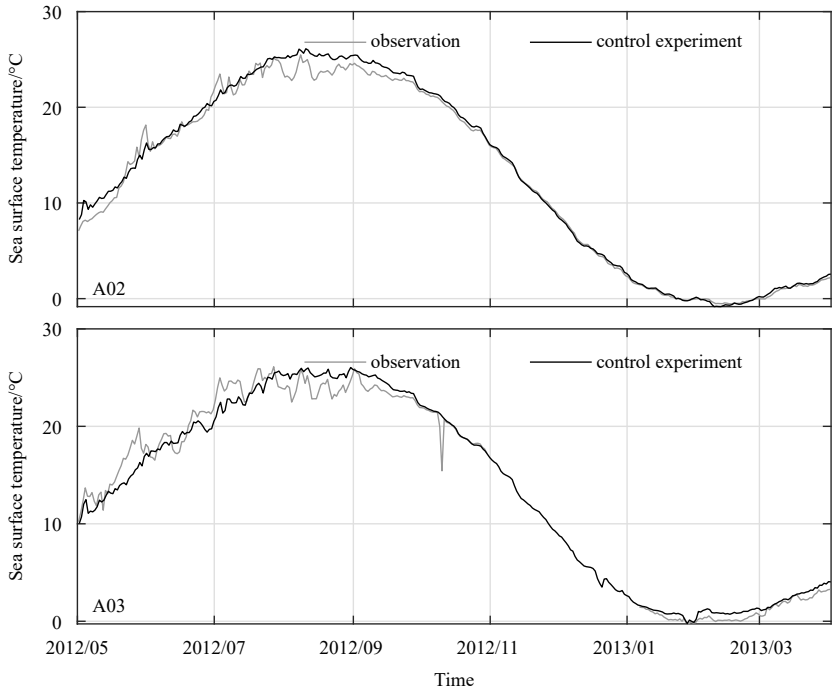

Fig. A3. Observed (grey lines) and modelled (black lines) sea surface temperature at three located marked by blue triangles in Fig. 1.

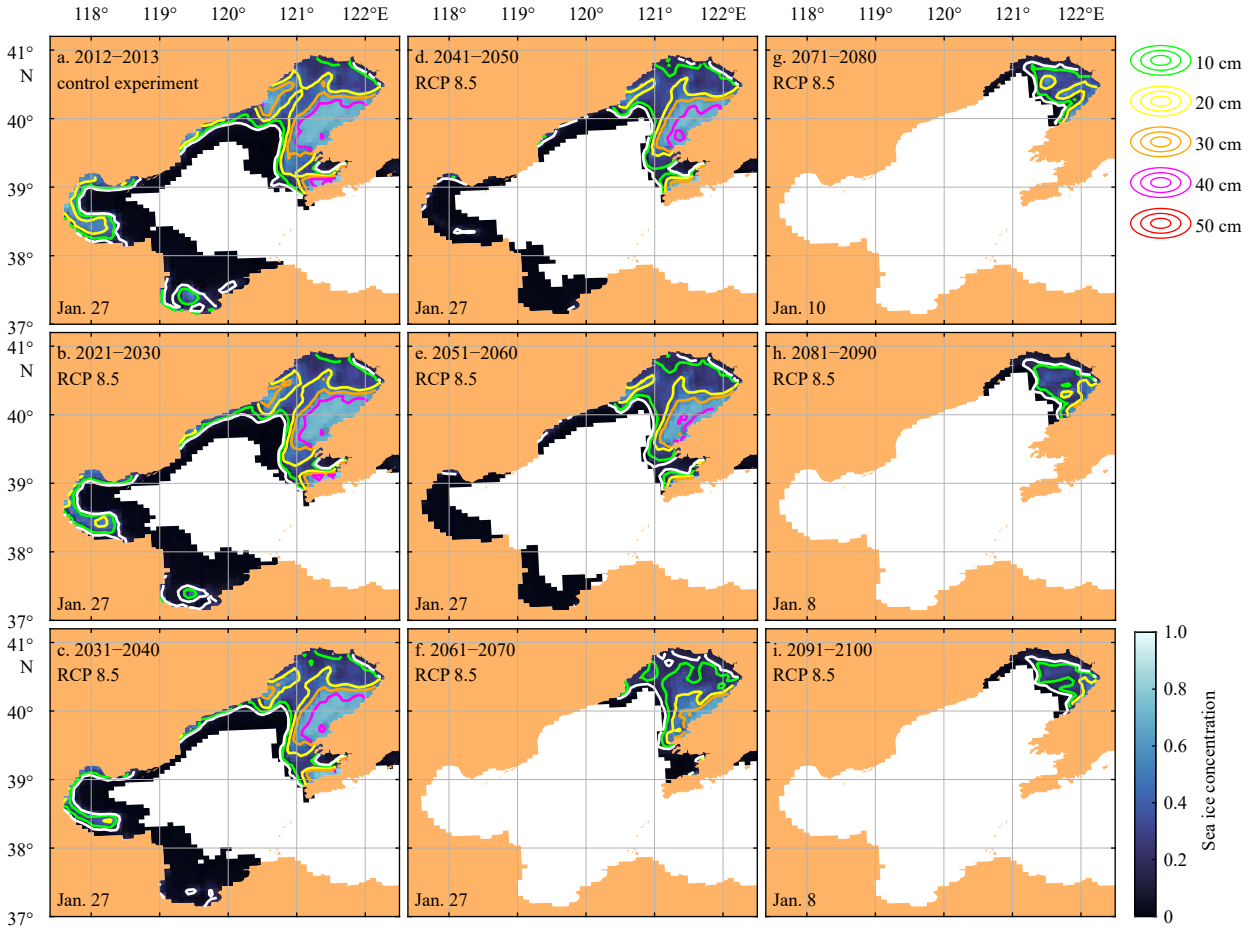

Fig. A4. Sea ice concentration (background color) and sea ice thickness (colorful contours) in the control experiment for the winter of 2012–2013 (a) and the sensitive experiments Exp-SE-a for the future in the RCP 8.5 scenario (b–i). The white contours indicate the 15% concentration of sea ice. Only the results with maximum sea ice extent in each experiment are shown.

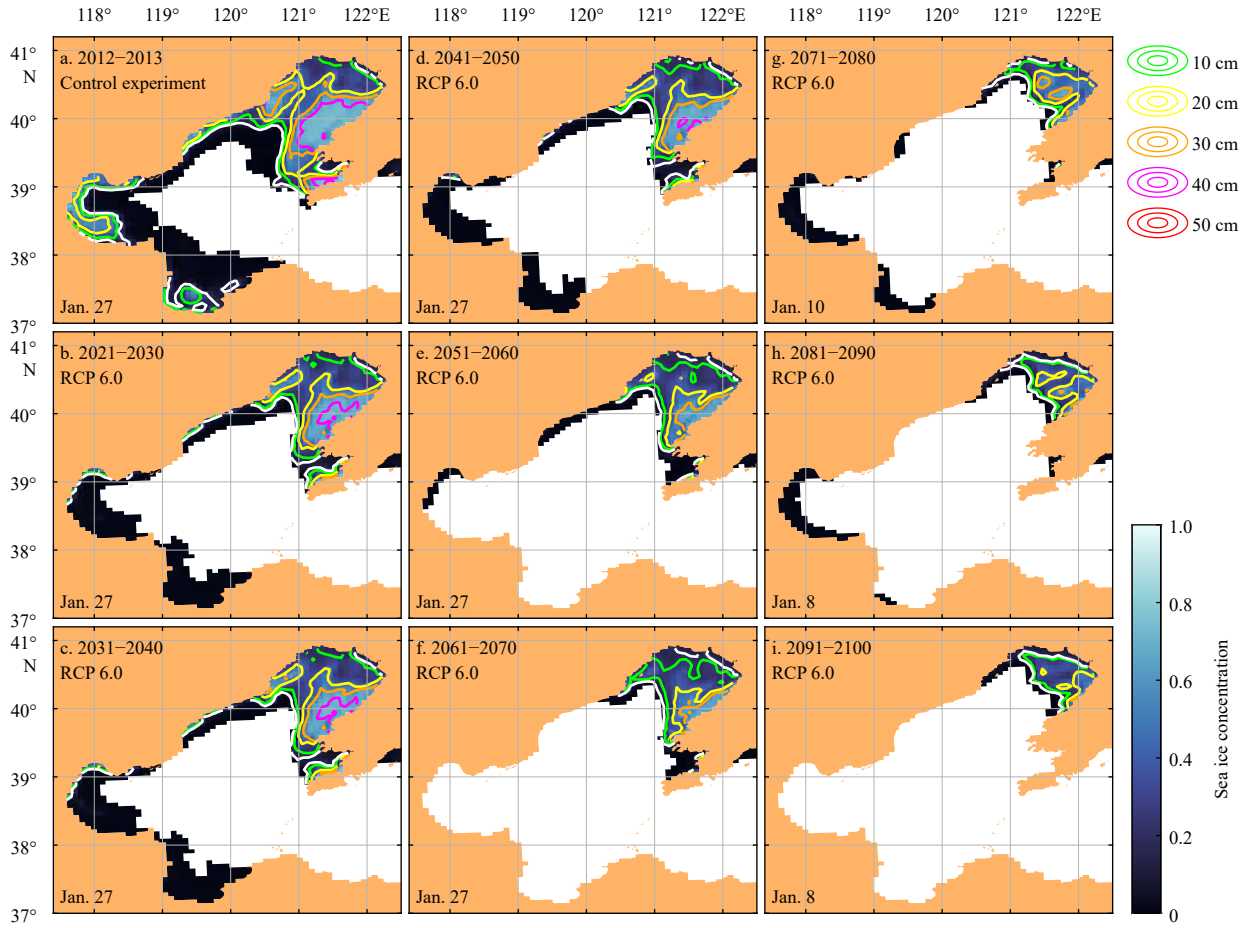

Fig. A5. Sea ice concentration (background color) and sea ice thickness (colorful contours) in the control experiment for the winter of 2012–2013 (a) and the sensitive experiments Exp-SE-a for the future in the RCP 6.0 scenario (b–i). The white contours indicate the 15% concentration of sea ice. Only the results with maximum sea ice extent in each experiment are shown.

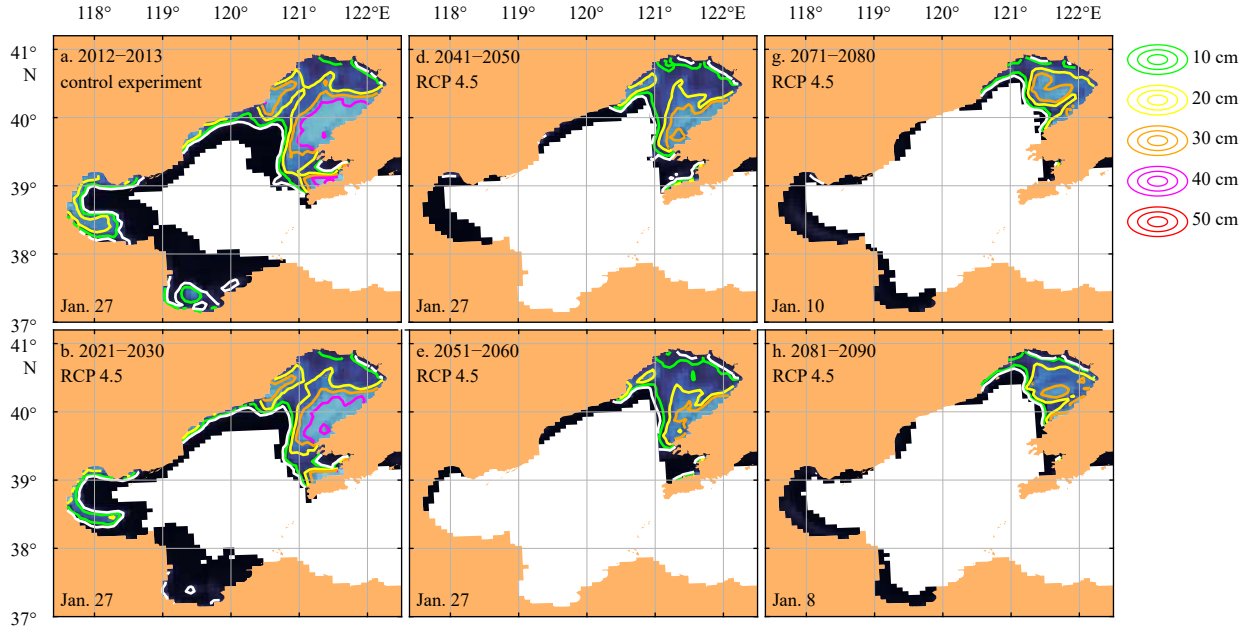

Fig. A6.

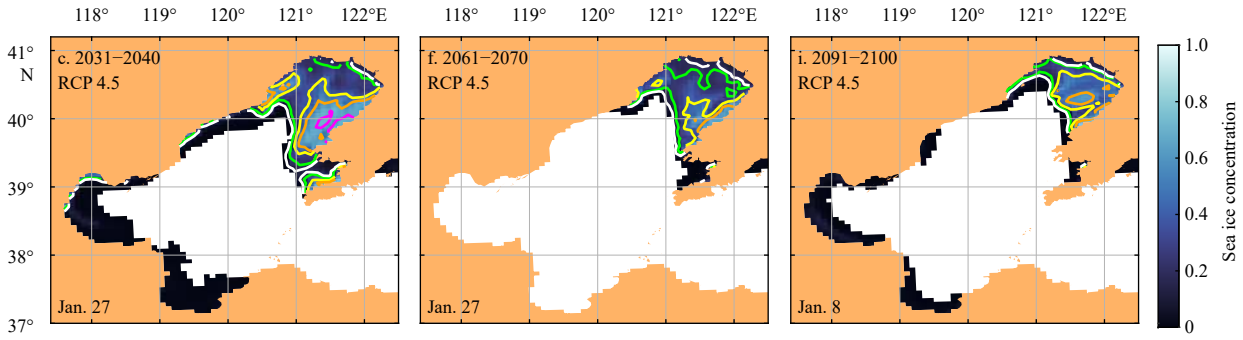

Fig. A6. Sea ice concentration (background color) and sea ice thickness (colorful contours) in the control experiment for the winter of 2012–2013 (a) and the sensitive experiments Exp-SE-a for the future in the RCP 4.5 scenario (b–i). The white contours indicate the 15% concentration of sea ice. Only the results with maximum sea ice extent in each experiment are shown.

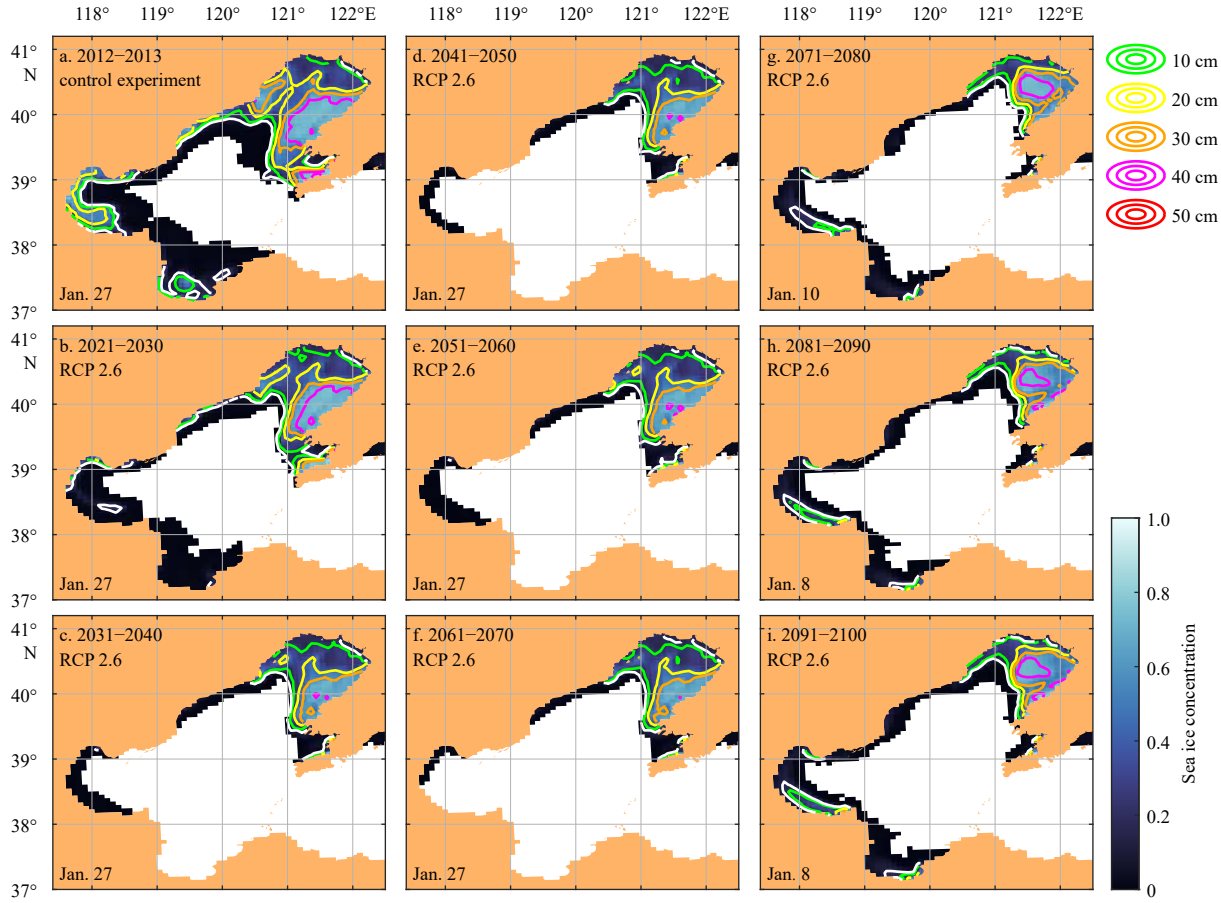

Fig. A7. Sea ice concentration (background color) and sea ice thickness (colorful contours) in the control experiment for the winter of 2012–2013 (a) and the sensitive experiments Exp-SE-a for the future in the RCP 2.6 scenario (b–i). The white contours indicate the 15% concentration of sea ice. Only the results with maximum sea ice extent in each experiment are shown.